North American Drought and Links to Northern Eurasia:

The Role of Stationary Rossby Waves

Hailan Wang[1], Siegfried D. Schubert, and Randal D. Koster

Global Modeling and Assimilation Office

NASA GSFC, Greenbelt, Maryland

April 2017

The AGU book "*Patterns of Climate Extremes: Trends and Mechanisms*"

[1] Also, Science Systems and Applications, Inc., Lanham, Maryland

Abstract

This chapter provides an overview of the role of stationary Rossby waves in the subseasonal development of warm season drought over North America and subsequent downstream development of climate anomalies over northern Eurasia. The results are based on a case study of a stationary Rossby wave event that developed during 20 May – 15 June 1988. Simulations with the NASA Goddard Earth Observing System (GEOS-5) atmospheric general circulation model highlight the importance of the mean jet streams in guiding and constraining the path and speed of wave energy propagation. In particular, convective anomalies that developed over the western Pacific in late May (in the presence of the strong North Pacific jet) produce a predilection for persistent upper-level high anomalies over central North America about ten days later, leading to the rapid development of severe dry conditions there. There are indications of continued downstream wave energy propagation that reaches northern Eurasia about two weeks later, leading to the development of dry conditions over eastern Europe and western Russia, and cool and wet conditions over western Europe and central northern Eurasia. The results suggest that stationary Rossby waves can serve as a source of predictability for subseasonal development of droughts over North America and northern Eurasia.

1. Introduction

A drought usually results from a prolonged period of below-normal precipitation in a given region. It can cause soil dryness and ground water shortage, and may contribute to wildfire, fatality, and even population migration. Because of its substantial impact on the agriculture and ecosystem of the affected regions, drought is one of the most expensive recurring natural disasters to affect North America and northern Eurasia. Within the U.S. alone, major droughts and heat waves during the last three decades have resulted in costs exceeding 100 billion dollars (Lott and Ross 2000; Ross and Lott 2003; Smith and Katz 2013). Take the 1988 North American drought for an example (Ross and Lott 2003). It not only caused severe damages to agriculture and related industries but also led to prolonged dust storms; it is also well known for extensive wildfires over western North America. Furthermore, the 1988 drought and its associated record-setting heat waves accounted for estimated 5,000 to 10,000 deaths. Ranked as the costliest drought in the U.S. history, the severe 1988 drought caused $60 billion (1988 United States dollars) in damage in the U.S., and additional $1.8 billion (1988 Canadian dollars) in Canada. The societal impact of droughts thus requires an advanced scientific understanding of processes that drive them, and a proper incorporation of these processes in forecast models in order to provide reliable drought prediction and drought early warning system to the society and policymakers.

The last few decades have seen significant advances in our understanding of the large-scale controls on droughts. For North America, it is now well established that certain spatial patterns of sea surface temperature (SST) anomalies are conducive to generating precipitation deficits or meteorological droughts there, achieved by exerting changes in atmospheric circulation there

through atmospheric tele-connection. Examples of such SST patterns include those associated with the El Niño Southern Oscillation (ENSO) on seasonal-to-interannual time scales and those associated with the Pacific Decadal Oscillation (PDO) and the Atlantic Multi-decadal Oscillation (AMO) on decadal and longer timescales (e.g., Schubert *et al.* 2009). Extensive observational (e.g., Ting and Wang 1997; Nigam *et al.* 2011; Hu and Feng 2012; Dai 2012) and AGCM modeling (e.g., Hoerling and Kumar 2003; Schubert *et al.* 2004; Seager *et al.* 2005; Schubert *et al.* 2009; Wang *et al.* 2010) studies show that ENSO and PDO in their cold phases and the AMO in its warm phase produce a tendency for drought conditions over the North America, with the Pacific playing the dominant role. It is also known that the impact of SST anomalies varies substantially from region to region. Droughts over the southern Plains and southwestern North America are significantly forced by certain tropical SST anomalies and appear to have some predictability on seasonal time scales, whereas droughts over the northern Plains and substantial areas of Canada are more strongly determined by atmospheric internal variability and appear less predictable (Hoerling *et al.* 2009; Seager and Hoerling 2014; Schubert *et al.* 2015). In addition, while certain SST patterns and random atmospheric internal variability can be important in initiating drought, sustaining and/or amplifying droughts over North America often involves feedback from local soil moisture (e.g. Koster *et al.* 2003; Ferguson *et al.* 2010). For example, a month with low precipitation leads to a drier-than-average soil which in turn can cause lower-than-average evaporation, helping to encourage low precipitation. Such feedback between land and atmosphere plays a particularly important role in sustaining droughts over central U.S. during the warm season (Koster *et al.* 2006). See Seager and Hoerling (2014) for a comprehensive overview of the atmosphere and ocean origins of North American droughts.

In northern Eurasia, precipitation and surface temperature variations on interannual time scales are not as strongly influenced by SST patterns; they are instead dominated by the effects of atmospheric internal variability (Schubert *et al.* 2015). Schubert *et al.* (2014), a review article on Northern Eurasian droughts and heat waves, found that some of the most severe summer heat waves and droughts are linked to distinct Rossby wave trains spanning the continent that, while producing severe heat in one location, cause a juxtaposition of wet and cool conditions in regions thousands of miles to the east or west. They note that longer-term droughts (lasting multiple years) do occur but are largely confined to the southern parts of northern Eurasia, where there appears to be a weak link to SST and an important control from soil moisture.

Despite significant progress made in understanding the processes that lead to droughts over North America and northern Eurasia, accurate drought predictions from weeks to a season in advance remain a challenge. While the role of SST anomalies for North American droughts has been extensively studied (as noted above), the SST impacts are often embedded in a substantial amount of atmospheric internal variability that is unforced by SST, limiting the potential predictability of precipitation over North America. The problem is even more significant in northern Eurasia where the connection to SST is much weaker, and thus drought prediction there poses an even greater challenge.

Summertime quasi-stationary Rossby waves are known to play a key role in Northern Hemisphere (NH) atmospheric circulation and surface meteorology variability on subseasonal time scales (Schubert *et al.* 2011; Schubert *et al.* 2014). In particular, such waves have been crucial to the development of recent short-term warm season heat waves and droughts over North America (e.g. the 1988, 1998 and 2012 summer droughts) and northern Eurasia (e.g., the 2003 summer heat wave over Europe and the 2010 summer drought and heat wave over Russia). For

example, past studies (e.g., Namias 1991; Chen and Newman 1998; Schubert et al. 2011) suggested that the intense anomalous upper-level anticyclonic flow anomalies associated with the 1988 drought are linked to quasi-stationary Rossby waves that originate from west Pacific.

The Rossby waves are guided by the mean jet streams (Branstator 2002; Schubert *et al.* 2011), as evidenced by the fact that the meridional gradients and nearly circumpolar extent of the warm season mean jet streams can provide important guides for Rossby waves (e.g. Ambrizzi et al. 1995). Stationary wave modeling diagnosis of leading patterns of summertime subseasonal atmospheric circulation variations shows that these waves are dominantly maintained by sub-monthly vorticity transient flux convergences (Schubert *et al.* 2011). Koster *et al.* (2014) further revealed that the leading subseasonal atmospheric circulation patterns over North America can be phase-locked and amplified by certain spatial patterns of soil moisture anomalies. The nature of these drought-inducing stationary Rossby waves, including physical processes that act to initiate and sustain them, is as yet not well understood.

This chapter provides an overview of the current understanding of the role of stationary Rossby waves in the development and maintenance of warm season drought over North America and northern Eurasia on subseasonal time scales. The study is also an extension of our previous work (Schubert *et al.* 2011; Koster *et al.* 2014) in that it further explores (via a case study) the processes by which stationary Rossby waves affect the subseasonal development of North American droughts, and their subsequent effects over northern Eurasia.

The chapter is organized as follows. Section 2 describes the reanalysis data and AGCM experiments. Section 3 presents our main results. Section 3.1 reviews the leading modes of subseasonal atmospheric circulation variability and their associated surface variations. Here we

update the results in Schubert *et al.* (2011) to include more recent years using NASA's Modern-Era Retrospective Analysis for Research and Applications (MERRA) (Rienecker *et al.* 2011) and MERRA-Land (Reichle *et al.* 2011) reanalysis data through 2014. Section 3.2.1 focuses on the 1988 North American drought, describing the key processes through which the stationary Rossby waves lead to the rapid buildup of severe drought conditions over central North America. Section 3.2.2 examines the connection between the subseasonal development of North American drought and the subsequent development of surface anomalies over northern Eurasia via stationary Rossby waves. The summary and conclusions are given in Section 4.

2. Reanalysis Data and the GEOS-5 AGCM Experiments

This study makes extensive use of daily and monthly atmospheric circulation and surface fields from recent reanalysis data: MERRA (Rienecker *et al.* 2011) and MERRA-Land (Reichle *et al.* 2011). MERRA was produced with the Goddard Earth Observing System Version 5 (GEOS-5) (Rienecker *et al.* 2008) consisting of the GEOS-5 Atmospheric General Circulation Model (AGCM) and the Grid-point Statistical Interpolation (GSI) analysis system. It was run at a resolution of ½° latitude × 2/3° longitude with 72 levels extending to 0.01hPa. MERRA-Land is an off-line land-only assimilation in which the precipitation forcing consists of a gauge-based data product from the NOAA Climate Prediction Center (CPC) merged with MERRA precipitation, and the land model is an updated version of the NASA GEOS-5 Catchment Land Surface Model. MERRA-Land has been shown to be more accurate than MERRA in terms of surface hydrological fields and is recommended for land surface hydrological studies (Reichle *et al.* 2011). More information about MERRA and MERRA-Land data can be found at https://gmao.gsfc.nasa.gov/research/merra/.

Our investigation focuses on the boreal summer months with much of the analysis based on monthly data. The subseasonal (30-90 day) component of the variability is obtained by first removing the annual cycle and then computing the departures of summer monthly anomalies from June-July-August (JJA) seasonal mean anomaly. In order to study the detailed evolution of stationary Rossby waves and the subseasonal development of regional climate extremes, we also make use of daily atmospheric circulation and surface temperature fields from MERRA and daily precipitation and surface soil wetness from MERRA-Land.

New results from this study are based on experiments performed with the NASA GEOS-5 AGCM (Rienecker *et al.*, 2008, Molod *et al.*, 2012), combined with a data assimilation technology called "replay" (described below). The GEOS-5 AGCM employs the finite-volume dynamics of Lin (2004) and various moist physics packages described in Bacmeister *et al.* (2006) including a modified form of the Relaxed Arakawa-Schubert convection scheme (Moorthi and Suarez, 1992), a prognostic cloud microphysics scheme (Bacmeister *et al.* 2006), and the Catchment Land Surface Model (Koster *et al.*, 2000). In our experiments, the model is run with 72 hybrid-sigma vertical levels extending to 0.01hPa and with 1° horizontal resolution on a latitude/longitude grid.

The GEOS-5 data assimilation system employed in MERRA was developed so that the analysis increments produced during the assimilation cycle are inserted gradually over a 6 hour interval into the model using the Incremental Analysis Updates (IAU) approach described in Bloom *et al.* (1996). This approach has been modified so that the model can be "replayed" against an existing analysis. The replay methodology reads in an existing analysis field (in this case MERRA) and mimics the IAU approach to provide a continuous model run that is forced by analysis increments

that change every 6 hours, thereby constraining the model to remain close to the original analysis. This approach has been generalized so that it allows us to constrain only certain components of the atmosphere (e.g., a limited region, or a subset of model variables).

Table 1 lists the AGCM experiments performed, focusing on the stationary Rossby wave event that occurred during 20 May – 15 June 1988. The experiments consist of two free-running AGCM hindcasts and two sets of AGCM regional replay experiments in which the constraint to MERRA is applied either over eastern Asia and the western Pacific (90ºE-140ºE, 0º-70ºN), or over North America (130ºW-70ºW; 0º-70ºN) (see Figure 8), while letting the model atmosphere evolve freely elsewhere.

Each of the experiments consists of two sets of ensembles: a control ensemble and an "anomaly" ensemble. The control ensemble consists of 31 hindcast runs forced with observed SST for the summers of 1980 through 2010 (one hindcast for each summer). The ensemble average of those runs is used to establish a hindcast climatology. The anomaly ensemble consists of 30 hindcast runs for the summer of 1988 forced with the 1988 observed SST. The atmospheric and land initial conditions used vary from experiment to experiment and are detailed below.

In the free-running AGCM hindcast experiment A1, the 31 members of the control ensemble are initialized at 21z 20 May in each of the years 1980-2010, using the atmospheric and land conditions for that date and time from MERRA. The 30 anomaly simulations are initialized at 21z 20 May 1988, just before the stationary Rossby waves develop in the observations, and run through the end of July 1988. The atmospheric initial conditions for the 30 anomaly ensemble members are obtained by adding small perturbations to the MERRA atmospheric state at 21z 20 May 1988; the land variables in all of the anomaly ensemble members are initialized with

MERRA land conditions at 21z 20 May 1988. Experiment A2 is the same as experiment A1 except that it uses MERRA atmospheric state at 21z 20 May of years 1980-2009 to initialize the atmosphere of its 30 anomaly members. The regional replay experiment B1 is the same as experiment A1 except that it constrains all of the model basic atmospheric variables to be close to those of MERRA over eastern Asia and the western Pacific (90ºE-140ºE; 0º-70ºN). Experiment B2 is the same as experiment B1 except that the initialization occurs in early May (21z 2 May) instead of 21z 20 May, and it uses MERRA atmospheric and land conditions for 21z 2 May of years 1980 through 2009 to initialize its 30 anomaly ensemble members for the summer of 1988. This is to remove most, if not all, of the effects of late May atmospheric and land initial conditions on the results, allowing the ensemble mean of B2 to highlight the effects of the stationary Rossby waves that originate from western Pacific. Experiment B3 is the same as experiment B2 except that it disables soil moisture feedback by continually resetting the soil moisture prognostic variables in the land model to seasonally varying climatological values. Experiment B4 is identical to experiment B2 except that it replays only the zonal and meridional wind over eastern Asia and western Pacific (90ºE-140ºE; 0º-70ºN); air temperature, atmospheric moisture, and surface pressure are allowed to evolve freely. Finally, experiment C1 is identical to B2 except that the MERRA-based replay of the atmospheric variables is only over North America (130ºW-70ºW; 0º-70ºN). We note that for each of the experiments, the control ensemble strictly follows the experimental design of the anomaly ensemble (e.g. dates of atmospheric and land initial conditions, replay region and variables, soil moisture feedback). Thus, among all the experiments performed, only A1 and A2 have identical control ensembles. The rest of the experiments differ from one another and also differ from A1/A2 in their control ensembles.

Experiment A1 is used to assess the GEOS-5 AGCM's ability to reproduce the stationary Rossby wave event of interest, and Experiment A2 is used to isolate the effect of the late May 1988 land initial conditions. The comparison between A1 and A2 thus highlights the contribution from the late May 1988 atmospheric initial conditions. Among the regional replay experiments, B1 offers the greatest potential to reproduce the stationary Rossby waves and their effects over North America, since it includes the most ingredients: the contributions from the late May 1988 atmospheric and land initial conditions, the observed stationary wave sources over the western Pacific, the (mostly) corrected model mean jet over the North Pacific (see Section 3.2), and soil moisture feedback over land. The examination of and comparison between experiments B1-B4 allow us to isolate and assess the relative contributions of these different ingredients to the evolution of the wave and its effects over North America. The experiment C1 is used to study the connections between surface anomalies over North America and northern Eurasia via stationary Rossby waves.

3. Results

3.1 The Leading Modes of Subseasonal Atmospheric Variability

To study subseasonal atmospheric circulation variations, we focus on 250-hPa meridional wind - a quantity that highlights wave activity in the upper troposphere. The leading patterns of subseasonal atmospheric circulation variability are extracted by performing rotated orthogonal function (REOF) analysis in which varimax rotation (e.g., Richman 1986) is used to separate the leading wave structures geographically. Figure 1 shows the top five leading patterns of subseasonal atmospheric circulation variability during boreal summer, obtained using a REOF analysis of MERRA 250-hPa intraseasonal monthly meridional wind anomalies over the NH for

June, July and August of 1980–2014. The 1st REOF explains 8% of the total variance and consists of a wave train pattern that appears to emanate from the northeastern coast of North America. The wave train pattern spans the North Atlantic and much of northern Eurasia north of the mean south Asian jet. The 2nd REOF is characterized by a wave train embedded in the North Atlantic jet. Over North America, it consists of (for the sign displayed here[2]) a northerly flow anomaly over the west and a southerly flow anomaly over the east, corresponding to an upper-level anticyclonic flow anomaly over the central North America. Further downstream at the North Atlantic jet exit, there are indications that the wave train (while weak) splits into two branches, with the northern branch spanning much of northern Eurasia and the southern branch embedded in the south Asian jet. The 4th REOF is similar overall to the 2nd REOF, except for a 90 degree phase shift and for being more confined to North America and the North Atlantic. The 3rd and 5th REOFs show similar wave trains confined to the North Pacific jet stream, distinguished primarily by a 90 degree phase shift. The 3rd REOF in particular has a notable component over North America where it shows a northerly flow anomaly to the west and a southerly flow anomaly to the east, corresponding to an anomalous upper-level high over the central U.S. Figure 1 clearly illustrates the importance of the mean summertime NH jet streams in guiding these leading subseasonal atmospheric circulation patterns.

These leading modes of subseasonal atmospheric circulation variability are associated with considerable subseasonal variations of surface meteorological fields (Figure 2). REOF1 is associated with notable surface temperature and precipitation anomalies over much of northern Eurasia, consisting of surface cooling and precipitation surpluses over southern Europe and

[2] Here and in the following, our descriptions of the REOF patterns and associated surface anomalies are based on the sign of the patterns displayed in Figure 1. The reader should keep in mind that the sign is arbitrary.

central Russia, accompanied by surface warming and precipitation deficits over eastern Europe. The surface anomalies associated with the REOF2 exhibit a wavetrain-like pattern spanning North America and northern Eurasia, with considerable surface warming and precipitation deficits over the central and eastern U.S., surface cooling and precipitation increases over much of the Europe, and surface warming and precipitation deficits near 60°E. The wave-train like pattern (Figure 2, second panels from top) suggests that these subseasonal surface anomalies over North America and northern Eurasia could be linked through the action of stationary Rossby waves – which we will explore in Section 3.2.2. By comparison, REOF4 primarily affects North America; it is associated with surface warming over western North America and cooling to the east, with notable precipitation deficits over central North America. Both REOF3 and REOF5 are associated with surface anomalies spanning the North Pacific. The REOF3 exhibits notable effects over North America: surface cooling over the Pacific Northwest and surface warming centered over the southern U.S., along with precipitation surpluses over northern U.S. and deficits over southern U.S. The REOF5 displays a moderate surface warming over Pacific Northwest and moderate surface cooling and precipitation increases over southern U.S. We note that these surface anomalies, which are based on MERRA and MERRA-Land data, are very similar to those based on the CRU TS3.0 (Harris et al. 2014) and GPCP (Adler et al. 2003) observations (not shown).

The subseasonal SST anomalies associated with the leading REOFs are vertically aligned such that warm (cold) SST anomalies lie beneath upper-level high (low) anomalies. This appears to reflect warm season air-sea interaction in the NH extratropical oceans where the rather shallow mixed layer allows a modest surface heat flux forcing from the overlying atmospheric circulation anomaly to exert considerable changes in mixed layer temperature, which in turn could feed back

onto the atmosphere, reinforcing the subseasonal atmospheric circulation anomaly. While not investigated here, there is observational evidence suggesting the importance of extratropical air-sea interaction for sustaining subseasonal atmospheric circulation anomalies (Peña *et al.* 2003; Wang and Lupo 2009).

In order to quantify the importance of the leading REOFs in accounting for subseasonal surface meteorological variations, we show in Figure 3 the fraction of the subseasonal variability of surface temperature and precipitation explained by the top ten leading REOFs. The leading REOFs primarily affect subseasonal surface variations over North America and northern Eurasia. They explain more than 60% of subseasonal surface temperature variations over much of central and northern U.S., Europe and western Russia, and more than 30% of subseasonal SST variations over the North Pacific and North Atlantic. The fraction of explained variance for precipitation is considerably smaller than that for surface temperature, with values exceeding 30% occurring primarily over the northern plains and Texas in North America as well as over northern Europe and western Russia.

3.2. The Influence of Stationary Rossby Waves on Drought

It is now well established that the leading modes of subseasonal atmospheric circulation variability play an important role in accounting for the subseasonal development of many regional climate extremes (Schubert *et al.* 2011). A better understanding of the causes and predictability of these climate extremes requires an exploration of the origin and predictability of stationary Rossby waves, as well as a study of the key processes through which these stationary waves lead to the climate extremes.

Here we focus on North America and northern Eurasia, the regions that appear to be most affected by the leading REOFs (Figure 3), by performing a case study of a drought event during which stationary Rossby waves play an important role. To select the drought event, we examine in Figure 4 the rotated principal components (RPCs) of the top five leading REOFs and focus our attention on the modes that strongly affect North America, i.e., REOF2 and REOF4. Among the drought events that occurred during the time period 1980-2014, the month of June 1988 stands out – it shows strong projections on both REOF2 and REOF4.

Figure 5 shows the monthly anomalies for June 1988. The 250-hPa meridional wind anomaly (Figure 5a) displays a wave-like pattern that appears to emanate from North America, crosses the North Atlantic, and then splits at the North Atlantic jet exit, with the northern branch extending eastward across much of northern Eurasia, and the southern branch confined to the south Asia jet. The anomalies have strong projections on both REOF2 and REOF4 over North America, and they resemble REOF2 over regions further downstream. The surface temperature anomalies (Figure 5b) over North America show strong surface warming of 8 degrees over central North America with cooling to the northeast. This is accompanied by a substantial precipitation deficit of -3 mm day^{-1} (Figure 5c) and surface soil dryness of -25% (Figure 5d) over the eastern portion of the U.S. The surface anomalies over northern Eurasia exhibit a wavetrain like pattern, with surface cooling, precipitation surpluses and soil wetness over southern Europe and central Russia, and surface warming and precipitation deficits along with surface soil dryness over western Russia. Overall, the surface temperature and precipitation anomalies for June 1988 (Figure 5b-c) show the combined contributions from REOF2 and REOF4 over North America as well as a prominent contribution from REOF2 over northern Eurasia (Figure 2). In addition,

there are regional SST anomalies of more than 1 degree over the North Pacific and North Atlantic, apparently reflecting the effects of extratropical air-sea interaction.

In order to better appreciate the stationary Rossby wave event(s) that occurred during June 1988 and the associated surface anomalies, we examine in Figure 6 the time evolution of the daily 250-hPa meridional wind and surface anomalies. Figure 6a clearly shows two stationary Rossby wave events that developed during 20 May – 15 June and 16 June – 8 July 1988. The energy associated with both waves propagates eastward from the North Pacific to western Eurasia, with the peak magnitude reached over North America. The wave event during 20 May – 15 June is particularly prominent. It appears to originate from the western Pacific, with the energy propagating across the North Pacific to North America where it reaches its peak magnitude and persists for about 3-4 weeks. While the stationary Rossby waves remain quasi-stationary over North America and affects surface conditions there, the wave energy slowly propagates further downstream across the North Atlantic, reaching Europe and western Russia about two weeks later; its magnitude meanwhile gradually weakens. The projections of daily 250-hPa meridional wind anomalies onto REOF2 and REOF4 (not shown) show that the first stationary Rossby wave event is dominated by REOF2, whereas the second is dominated by REOF4. This explains the aforementioned strong projections of the monthly mean anomalies for June 1988 on both REOF2 and REOF4 (Figure 4). This also emphasizes the necessity of using daily data to study the waves and their effects on the development of regional surface anomalies.

Strong local surface anomalies develop rather quickly (Figure 6b, 6c, 6d) as soon as the stationary Rossby waves are established over North America and northern Eurasia. In particular, surface warming, precipitation deficit and surface soil dryness anomalies over both continents

develop within 1-2 days under the overlying upper-level anticyclonic flow associated with the stationary Rossby waves. The amplitudes of the surface anomalies over northern Eurasia are overall weaker than those over North America. Figure 6c-d shows that, while central North America is already experiencing precipitation deficits and surface soil dryness in early and mid-May, the sustained extreme precipitation deficits and surface dryness from late May through much of June 1988, presumably linked to the stationary Rossby waves, are much more distinct. In comparison, the surface anomalies over northern Eurasia appear to develop only after the stationary Rossby waves arrive, implying that these anomalies are initiated and then maintained by the waves. Furthermore, associated with the eastward wave energy propagation from North America to western north Eurasia, the surface anomalies over northern Eurasia occur about two weeks after those over North America. This suggests that surface anomalies in North America and Eurasia may be linked via stationary Rossby waves. We will explore this further in Section 3.2.2.

Based on the examination of Figure 6, we choose the 20 May – 15 June 1988 stationary Rossby wave event as the case study for our investigation. It is used to study the processes by which stationary Rossby waves are established over North America and lead to the quick buildup of severe drought conditions there. This case study also allows us to examine potential connections, via stationary Rossby waves, between North American drought and subsequent surface anomalies over northern Eurasia.

We use AGCM modeling in our analyses because it allows us to isolate and assess the key processes that affect stationary Rossby waves and associated regional climate extremes. An inspection of the warm season mean NH jet in the GEOS-5 AGCM, however, shows that while

the simulation of the north Atlantic jet is generally reasonable, the model is deficient in simulating the North Pacific jet (Figure 7b). The North Pacific mean jet in the GEOS-5 AGCM (Figure 7b) is considerably weaker and less organized than the observed as estimated from MERRA (Figure 7a) – a deficiency also seen in many other current AGCMs (not shown). The poor simulation of the North Pacific jet limits the usefulness of the free-running GEOS-5 AGCM for this study.

We use the "replay" technology to circumvent this model bias. We first determine the region that provides the forcing for the mean North Pacific jet by performing several regional replay experiments in which the model atmosphere is constrained over various regions upstream of the jet (not shown). The results show that the air temperature over central and north Asia and the diabatic heating over eastern Asia and western Pacific (90ºE-140ºE; 0-70ºN) (Figure 8) play a key role in maintaining the North Pacific jet, in part through thermal wind balance. Constraining the GEOS-5 model atmosphere to be close to MERRA over this region (experiment B2) brings the simulated jet (ensemble average of 250-hPa zonal wind in the control ensemble of B2) close to the observed jet (compare Figures 7a and 7c). In experiment B2, the simulated mean jet is in the correct location, with the correct shape and magnitude over much of the North Pacific; only minor biases are still seen over the northeastern Pacific, where the model jet is still somewhat weak. Furthermore, since the stationary Rossby wave event of interest originates from convective anomalies over the western Pacific (Chen and Newman 1998), the locally replayed region (Figure 8) in experiment B2 is appropriate. Given the improved jet and the utilization in replay mode of the observed locality of the Rossby wave sources, experiment B2 provides a useful framework for a study of wave propagation across the North Pacific and the subsequent effects on drought development over North America.

We also evaluate the mean North Pacific jet in the other regional replay experiments. The jet produced in experiment B1 (not shown) is similar to that in experiment B2, which is expected because the atmospheric and land initial conditions at 21z 20 May only affect the following two weeks and thus have little impact on the JJA mean jet. The mean NH jet in B3 (not shown) also resembles that in B2, suggesting a minor impact of soil moisture feedback on the mean jet. In contrast, constraining only the zonal and meridional wind fields over the region 90ºE-140ºE; 0-70ºN (experiment B4) produces a North Pacific mean jet with the correct location and shape but with considerably weaker amplitude over the central and eastern North Pacific (Figure 7d); deficiencies and biases associated with atmospheric variables not constrained in B4 (e.g., air temperature and specific humidity) are apparently able to feed back onto the zonal and meridional winds, leading to considerably larger analysis increments for zonal wind in B4 than in B2 which subsequently affects the mean North Pacific jet downstream. Note that a comparison between B2 and B4 allows us to assess the impact of the magnitude of the mean North Pacific jet on wave energy propagation across the North Pacific and subsequent conditions over North America.

The examination of the NH mean jet in experiment C1 (Figure 7e) shows that constraining the model atmosphere to be close to MERRA over North America (Figure 8) leads to moderate improvements over North America, where the model jet strengthens by about 5 m s^{-1} and is placed slightly southward. There are, however, still moderate differences over western north Eurasia, where the model underestimates the mean zonal wind by about 5 m s^{-1}.

3.2.1. The 1988 North American Drought

In this subsection, we first assess the skill of the GEOS-5 AGCM in reproducing the stationary Rossby wave event of interest; we then investigate the key factors that influence stationary Rossby waves and their effects over North America. Figure 9 and Figure 10 show the stationary Rossby waves produced in the two free-running GEOS-5 AGCM hindcast experiments (A1 and A2), the regional replay experiments B1 through B4, and nature (MERRA). The atmospheric circulation anomalies over North America in MERRA during 20 May – 15 June are overall quasi-stationary (Figure 9a); they consist of a distinct northerly flow anomaly over western North America and a southerly flow anomaly over eastern North America (Figure 10a), corresponding to an upper-level positive height anomaly over central North America. The free-running GEOS-5 AGCM hindcast from A1 (Figure 9b) shows rather limited skill beyond 1 week, after which the circulation anomalies show notable retrograde (westward) motion rather than remaining quasi-stationary as in MERRA (Figure 9a), a reflection of the weak mean zonal jet in the free-running model (Figure 7b). Consequently, the circulation anomalies in experiment A1 are opposite to those in MERRA in early June (Figure 9b). The mean atmospheric circulation anomalies over North America for experiment A1 averaged over 26 May – 10 June 1988 are displaced westward relative to those in MERRA, with a northerly flow anomaly over northwest North America and a southerly flow anomaly over central North America (Figure 10b). The spread between the ensemble members is modest overall (Figure 10c), due to the imposition of the 21z 20 May 1988 atmospheric and land initial conditions. The free-running GEOS-5 AGCM hindcast that makes use only of MERRA land initial conditions at 21z 20 May 1988 (A2) essentially shows no skill in producing the observed stationary Rossby waves (Figure 9c, Figure 10d), with rather large intra-member spread (Figure 10e). The contrast between A1 and A2

highlights the importance of the late May atmospheric initial state for the AGCM hindcast; the contribution from the late May dry land initial condition is minor.

While not shown here, we also examined the contribution of SST anomalies to the AGCM hindcast by performing two other AGCM hindcast experiments that are the same as A1 and A2 but using climatological SST (1980-2010). The results from these hindcast experiments are similar overall to those from A1 and A2, indicating that the SST anomalies played a very minor (if any) role in forcing the anomalies that occurred over North America during the period 20 May – 15 June 1988 (not shown).

As discussed earlier, experiment B1 includes all of the key factors considered in our experiments: the observed stationary Rossby wave sources over the western Pacific, a mostly corrected North Pacific mean jet, the atmospheric and land initial conditions in late May, and soil moisture feedback over land. This combination results in a significantly improved reproduction of the Rossby wave event of interest (Figure 9d, Figures 10f-g; focus on the case study period of 20 May – 15 June). In fact, among all the regional replay experiments, B1 shows the strongest agreement with MERRA. The circulation anomalies in the ensemble mean of B1 strongly resemble those of MERRA over the North Pacific as well as North America (Figure 9d, Figure 10f). The ensemble spread among the 30 members gradually increases as the wave energy propagates away from the replay region (Figure 10g). Over North America, most of the 30 ensemble members agree with their ensemble mean in producing a northerly flow over western North America and a southerly flow over eastern North America. There are indications of a slight lagging of the waves in B1 relative to MERRA over the northeast Pacific and western North America (Figure 10g), which could be due to the modestly weaker simulated jet there

(Figure 7c). The considerable improvement in B1 over A1 confirms that the stationary wave sources reside in the western Pacific. By comparison, the stationary Rossby event during 16 June – 8 July 1988 is not captured in the ensemble mean of B1, suggesting that these waves could originate from processes outside the replay region (90ºE-140ºE; 0º-70ºN).

The results from B2 are similar overall to those from B1 except that they have moderately smaller amplitudes due to the modestly larger ensemble spread (Figure 9e, Figure 10h-i), and that they displace the circulation anomalies westward relative to MERRA in late May, due to the lack of constraints from late May initialization. It is worth noting that despite the diverse atmospheric and land initial conditions used in the anomaly runs, most of the 30 ensemble members agree with MERRA in showing a northerly flow anomaly over western North America and a southerly flow anomaly over eastern North America (Figure 10i). This suggests that with a mostly corrected North Pacific mean jet, the observed stationary wave sources in the western Pacific do provide a predilection for persistent upper-level anticyclonic flow anomalies over central North America about one to two weeks later.

The results from B3 (Figure 9f, Figure 10j-k) are in strong agreement with those from B2, with only a modestly smaller ensemble spread over North America and regions further downstream. The overall good agreement between B3 and B2 suggests that during the period (3-4 weeks) in which the stationary Rossby waves existed over North America, local soil moisture variations induced by the wave did not significantly feedback on the overlying upper-level atmospheric circulation anomalies.

The results from B4 (Figure 9g, Figure 10l-m), the experiment that constrains only the winds through the replay approach, distinctly differ from those of B2 (Figure 9e, Figure 10h-i). While

B4 is similar to B2 in prescribing the observed stationary wave sources over the western Pacific, the mean jet over the North Pacific (Figure 7d) is considerably weaker than that in B2 (Figure 7c) east of the dateline, thus imposing a weaker constraint on wave propagation there. As a result, B4 shows a slower eastward propagation and a larger ensemble spread east of dateline than B2 (compare Figure 10m and Figure 10i); the ensemble mean of B4 over North America not only shows a rather weak magnitude but also places the responses in the wrong locations (Figure 10l).

Upon their establishment over North America, the stationary Rossby waves exert a strong impact on the local fields. MERRA (Figure 11a-c) shows that during the late May – middle June stationary Rossby wave event, there are distinct surface warming anomalies over central North America and strong precipitation deficits and surface dryness over central and eastern America. The 26 May – 10 June mean surface anomalies in the AGCM hindcast (experiment A1) (Figure 11d-f) are somewhat similar to MERRA except that the anomalies are weaker in magnitude and are also shifted westward due to the westward displacement of upper-level atmospheric circulation anomalies (Figure 9b). The isolated impact of the late May land initial conditions on the surface temperature and precipitation anomalies over North America is rather weak (Figure 11g-h), consistent with the weak atmospheric circulation anomalies in A2 (Figure 9c, Figure 10d-e). The ensemble mean surface anomalies in experiment B1 (Figure 11j-l) show the best agreement with those in MERRA (Figure 11a-c), benefiting from a good reproduction of the observed stationary Rossby waves over North America (Figure 9d, Figure 10f-g). The strong surface soil dryness anomalies in A1, A2 and B1 mainly reflect the late May 1988 dry land initial condition.

The ensemble mean surface anomalies in B2 (Figure 11m-o) are similar overall to those in B1, except that magnitudes are reduced by 50% for surface temperature and precipitation and by considerably more for surface soil wetness, since unlike B1, B2 does not benefit from a dry land initialization in late May. The surface anomalies in B2 essentially reflect the effects of the overlying quasi-stationary upper-level high anomalies that originate from the stationary Rossby wave sources over western Pacific.

Disabling soil moisture feedback in B3 only modestly affects the precipitation anomalies over the central and eastern U.S. (compare Figure 11n and Figure 11q), but does have moderate impact on surface temperature anomalies. The magnitude of surface warming response over central North America in B3 (Figure 11p) is about 60% of that in B2 (Figure 11m), suggesting soil moisture feedback contributes to about 40% of surface warming in B2.

The results of experiment B3 (Figure 9f, Figure 10j-k, Figure 11 p-r) may at first glance seem counter to the findings of Koster *et al.* (2014), who found a significant impact of soil moisture anomalies on such waves. Note, however, that Koster *et al.* (2014) studied a very different problem: how the imposition of large soil moisture anomalies may affect the atmospheric circulation. In B2, initial soil moisture conditions were not extreme on average, and while some soil moisture anomalies are generated in B2 over the course of the simulations, they are not especially large (compare Figures 11c,o). Comparing B3 with B2 therefore does not address the question of how large soil moisture anomalies may influence wave structure. More germane to the Koster et al. (2014) study are the results of A2, which does impose a strong soil moisture anomaly. Here we can only speculate on why the wave response is smaller in A2 than in Koster et al. (2014). One potential explanation involves the spatial breadth of the imposed soil moisture

anomaly in A2 – as indicated in a map of the initial soil moisture anomaly (not shown) and as implied in Figure 11i, the initial soil moistures in both the southern Great Plains and the northwest U.S. were anomalously dry in A2, which would lead (according to the results of Koster et al. [2014]) to conflicting impacts on the nature of the overlying wave. That is, the impacts of the southeastern and northwestern dry soil moisture anomalies in A2 may, in this case, have partially canceled each other out.

While both B2 and B4 prescribe the observed stationary Rossby wave sources over the western Pacific, the surface anomalies in the latter (Figure 11s-u) are weak overall and show little resemblance to MERRA, due to the poor simulation in B4 of atmospheric circulation anomalies over North America (Figure 9g, Figure 10 l-m) stemming from the simulation of a weak North Pacific mean jet east of the dateline (Figure 7d). The contrast between B2 and B4 illustrates the importance for a model to correctly simulate the North Pacific mean jet, not only its latitudinal location and shape but also its magnitude, so as to let the wave energy propagate across the North Pacific with the correct speed and direction and subsequently exert the correct regional effects over North America. Since it usually takes one to two weeks for the wave energy to propagate across the North Pacific, knowledge of western North Pacific sources for stationary Rossby waves can serve as a potential source of predictability for North American droughts.

3.2.2. North American Drought and Surface Anomalies over Northern Eurasia

Observations (Figure 2, Figure 5, Figure 6, Figure 12a) imply that subseasonal surface anomalies over North America and those over northern Eurasia may be connected to each other via stationary Rossby waves. Observed surface anomalies in northern Eurasia, however, are often strongly influenced by local processes that may mask out the effects of such waves (e.g.,

Schubert *et al.* 2014). Here we address these issues by performing a regional replay experiment in which the GEOS-5 model atmosphere is constrained to be close to MERRA over North America (experiment C1) and then studying what occurs downstream.

The ensemble mean 250-hPa meridional wind in C1 (Figure 12b) shows that while the strong quasi-stationary atmospheric circulation anomalies remain over North America (as necessitated by the replay design) leading to the severe drought conditions there, there are indications in C1 of wave energy propagation downstream under the guiding effect of the North Atlantic jet, reaching Europe and western Russia about two weeks later. In particular, off the North Atlantic jet exit, the ensemble mean shows a distinct wave train propagating eastward along the northern edge of northern Eurasia (Figure 12d). The model ensemble spread (Figure 12e) over the North Atlantic is strongly constrained by the strong North Atlantic jet and then increases notably off the jet exit where the upper zonal wind weakens markedly. The majority of the ensemble members consistently show a southerly flow anomaly off the west coast of Europe, a northerly flow anomaly over central Europe, and a southerly flow anomaly further downstream over central northern Russia. The wavetrain-like responses over Europe and northern Russia in the ensemble mean are displaced somewhat north of those of MERRA (Figure 12c), possibly due to the underestimation of the mean zonal wind there (by about 5 m s^{-1}).

The stationary Rossby waves over northern Eurasia affect the local surface conditions considerably (Figure 13). The upper-level anticyclonic flow anomalies associated with the stationary Rossby waves act to both warm and dry the atmosphere and land surface, leading to local surface warming, precipitation deficits and soil moisture dryness, whereas the upper-level cyclonic flow anomalies exert surface anomalies of the opposite sign (Figure 13b, d, f). Relative

to the observations (Figure 13a, c, e), the model surface anomalies are displaced northward, consistent with the northward displacement of the model-produced stationary Rossby waves (Figure 12d).

Despite the noted model biases, experiment C1 provides evidence that stationary Rossby waves (resembling REOF2) that lead to drought over central North America can subsequently affect northern Eurasia. They can provide a predilection for dry conditions to develop over eastern Europe and western Russia and for cool and wet conditions to develop over both western Europe and central northern Russia.

The fact that the surface anomalies over northern Eurasia lag those over North America by about two weeks has important implications for subseasonal forecasts in Europe and western Russia. Improved prediction skill for weeks 3-4 can potentially be realized if the forecast model used properly represents stationary Rossby wave generation over North America, the wave energy propagation across the North Atlantic (requiring a realistic simulation of the North Atlantic jet), and the subsequent stationary Rossby wave impacts over northern Eurasia.

While our investigation here focuses on the 20 May – 15 June 1988 stationary Rossby wave event which appears to originate from convective processes over the western Pacific, we note that any stationary Rossby waves over North America, regardless of how they are initiated and sustained, can subsequently lead to subseasonal surface anomalies over Europe and western Russia. For example, using a series of idealized AGCM experiments, Koster *et al.* (2014) obtained an REOF2-like atmospheric circulation pattern over North America by imposing a persistent dry soil moisture anomaly over the central U.S. and a persistent wet soil moisture anomaly over the northwestern U.S. As the wave energy is propagated downstream, the model

ensemble mean exhibits a wavetrain-like pattern over Europe and western Russia (Figure 14) that is somewhat similar to that in experiment C1 (Figure 12d).

4. Summary and Conclusions

The leading modes of subseasonal atmospheric circulation variability play an important role in determining subseasonal surface meteorological variations during the warm season, and they have been crucial in the development of many recent short-term warm season climate extremes over North America and northern Eurasia. These leading modes are guided by the NH mean jet streams and are maintained by sub-monthly transients (Schubert *et al.* 2011). There is evidence that subseasonal atmospheric circulation anomalies over land can be phase-locked and amplified by certain spatial patterns of soil moisture anomalies (Koster *et al.* 2014).

Using the NASA GEOS-5 AGCM and a data assimilation technology called "replay", we perform a case study of the 20 May – 15 June 1988 stationary Rossby wave event. Through this case study, we systematically investigate the processes through which stationary Rossby waves lead to the development of the severe 1988 drought conditions over central North America which subsequently influence surface anomalies over northern Eurasia. In particular, we perform a series of AGCM experiments designed to isolate the contributions to this event from: (i) atmosphere and land initial conditions in late May 1988, (ii) observed stationary wave sources over the western Pacific, (iii) the correct simulation of the model mean jet over the North Pacific, and (iv) soil moisture feedback over land.

While the free-running GEOS-5 AGCM provides a generally reasonable simulation of the warm season North Atlantic jet, it is deficient in simulating the North Pacific mean jet; the model

North Pacific jet is considerably weaker and less organized than the observed. This model deficiency significantly affects the simulation and hindcasts of stationary Rossby waves and their effects over North America and northern Eurasia, and thus limits the usefulness of the free-running GEOS-5 AGCM for this study. To circumvent this deficiency, we perform a series of regional "replay" experiments in which the GEOS-5 model atmosphere is constrained to be close to MERRA over eastern Asia and the western Pacific. This constraint indeed allows the GEOS-5 AGCM to produce a greatly corrected North Pacific mean jet, providing us with a useful modeling framework for our analysis.

Our modeling results show the crucial importance of the strong mean jet streams over the North Pacific and North Atlantic for guiding and constraining wave energy propagation path and speed and thereby providing a potential source of predictability. For the 20 May – 15 June 1988 stationary Rossby wave event investigated here, the free-running model hindcast skill is limited to only about one week, beyond which the hindcasted waves show westward retrograde displacement instead of remaining quasi-stationary as in the observations, due to the weak mean jet over the North Pacific. With the mostly corrected (through replay) North Pacific mean jet, our results show that convective anomalies over the western Pacific do produce a predilection for sustained upper-level high anomalies over central North America about one to two weeks later. Such high anomalies subsequently lead to strong local precipitation deficits, soil dryness and surface warming, and thereby to severe drought conditions there. For the period that the stationary Rossby waves remain over North America, local soil moisture anomalies induced by the waves amplify the temperature effect somewhat but do not appear to feed back noticeably on the waves and the precipitation.

While the stationary Rossby waves over North America lead to local drought conditions, there are indications of wave energy propagation further downstream under the waveguiding effect of the North Atlantic jet. This results in the establishment of stationary Rossby waves over Europe and western Russia about two weeks later, facilitating (for this case) drought conditions over eastern Europe and western Russia, and cool and wet conditions over western Europe and central northern Eurasia.

Since it usually takes about two weeks for the wave energy to propagate across the North Pacific (North Atlantic) to reach North America (northern Eurasia), these waves can potentially serve as a source of subseasonal forecast skill in these downstream locations. To access this skill, however, it would be critically important for a forecast model to correctly simulate the mean NH jet streams, not only their location and shape but also their magnitude, in order to allow the correct simulation of wave propagation (path and speed) across the northern oceans.

While this study focuses on the summer 1988 drought, the modeling approach employed here can similarly be applied to other climate extremes involving stationary Rossby waves. In addition, since the weak mean jet bias over the North Pacific in the GEOS-5 AGCM is also seen in many other current models, drought studies using these other AGCMs may find our "replay" approach useful.

A number of key research challenges remain. First, the predictability of stationary Rossby waves is unclear and needs to be assessed. This requires an identification of the processes that initiate stationary Rossby waves and an assessment of their predictability. The origins of stationary Rossby waves could vary from event to event. While some stationary Rossby waves originate from regional subseasonal SST variations and thus possess certain predictability, others could be

generated by pure atmospheric internal variability and are hence unpredictable. The origins of stationary Rossby waves need to be further investigated by analyzing past events using observations and reanalyses. In addition, the processes that potentially sustain the stationary Rossby waves, including extratropical air-sea interaction and local land soil moisture feedback, also need to be better understood. Second, possible interaction between the short-term stationary Rossby waves and climate variations on decadal and longer time scales needs focused study (Schubert *et al.* 2014). There is, for example, considerable evidence that PDV, AMV, and global warming can play important roles in the occurrence of long-term drought (e.g., McCabe *et al.* 2004; Cook *et al.* 2015; Schubert *et al.* 2015), yet the possibility that such long-term changes might impact stationary Rossby waves and short term drought development (e.g., through changing the mean jet streams) is yet to be addressed. Third, to incorporate properly the effects of stationary Rossby waves, current models need to be considerably improved, or at least artificially corrected, to provide a correct representation of the NH mean jet, as well as to represent properly the processes that initiate and sustain stationary Rossby waves (e.g., soil moisture feedback over land). The proper representation of stationary Rossby waves in a model provides hope for considerably improved subseasonal drought forecast skill. This is of particularly high practical importance, for example, for operational drought outlooks.

Acknowledgments

This study is supported by the NOAA Climate Program Office Modeling, Analysis, Prediction, and Projections (MAPP) program.

References

Adler, R. F., and Coauthors, 2003: The version 2 Global Precipitation Climatology Project (GPCP) Monthly Precipitation Analysis (1979–present). *J. Hydrometeor*., **4**, 1147–1167.

Ambrizzi, T., B. J. Hoskins, and H.-H. Hsu, 1995: Rossby wave propagation and teleconnection patterns in the austral winter. *J. Atmos. Sci*., **52**, 3661–3672.

Bacmeister, J. T., M. J. Suarez, and F. R. Robertson, 2006: Rain reevaporation, boundary layer–convection interactions, and Pacific rainfall patterns in an AGCM. *J. Atmos. Sci*., **63**, 3383–3403.

Bloom, S., L. Takacs, A. DaSilva, and D. Ledvina, 1996: Data assimilation using incremental analysis updates. *Mon. Wea. Rev*., **124**, 1256–1271.

Branstator, G., 2002: Circumglobal teleconnections, the jet stream waveguide, and the North Atlantic Oscillation. *J. Climate*, **15**, 1893–1910.

Chen, P., and M. Newman, 1998: Rossby wave propagation and the rapid development of upper-level anomalous anticyclones during the 1988 U.S. drought. *J. Climate*, **11**, 2491–2504.

Cook, B.I., T.R. Ault, and J.E. Smerdon, 2015: Unprecedented 21st-century drought risk in the American Southwest and Central Plains. *Sci. Adv.*, **1**, no. 1, e1400082, doi:10.1126/sciadv.1400082

Dai, A., 2013: The influence of the Inter-decadal Pacific Oscillation on U.S. precipitation during 1923-2010. *Climate Dynamics*, **41**, 633–646.

Ferguson, Ian M., John A. Dracup, Philip B. Duffy, Philip Pegion, Siegfried Schubert, 2010: Influence of SST Forcing on Stochastic Characteristics of Simulated Precipitation and Drought. *J. Hydrometeor*, **11**, 754–769.

Harris, I., Jones, P.D., Osborn, T.J. and Lister, D.H. (2014), Updated high-resolution grids of monthly climatic observations – the CRU TS3.10 Dataset. *Int. J. Climatol*., **34**, 623–642.

Hoerling, M.P. and A. Kumar, 2003: The perfect ocean for drought. *Science*, **299**, 691-699.

Hoerling, M., X.W. Quan, and J. Eischeid, 2009: Distinct Causes for Two Principal U.S. Droughts of the 20th Century. *Geophys. Res. Lett.*, **36**, L19708, doi:10.1029/2009GL039860.

Hu, Qi, Song Feng, 2012: AMO- and ENSO-Driven Summertime Circulation and Precipitation Variations in North America. *J. Climate*, **25**, 6477–6495.

Koster, R. D., M. J. Suarez, and M. Heiser, 2000: Variance and predictability of precipitation at seasonal-to-interannual timescales. *J. Hydrometeor*., **1**, 26–46.

Koster, R. D., M. J. Suarez, Higgins, R. W., and H. M. Van den Dool, 2003: Observational evidence that soil moisture variations affect precipitation. *Geophys. Res. Lett*., **30**, 1241, doi:10.1029/2002GL016571.

Koster, R. D., Z. Guo, P. Dirmeyer, and 23 others, 2006: GLACE, The global land-atmosphere coupling experiment, 1, Overview. *J. Hydrometeorology*, **7**, 590-610.

Koster D. Randal, Yehui Chang, and Siegfried D. Schubert, 2014: A Mechanism for Land–Atmosphere Feedback Involving Planetary Wave Structures. *J. Climate*, **27**, 9290–9301.

Lin, S.-J., 2004: A ‘‘vertically Lagrangian’’ finite-volume dynamical core for global models. *Mon. Wea. Rev*., **132**, 2293–2307.

Lott, N., and T. Ross, 2000: A Climatology of Recent Extreme Weather and Climate Events. Technical Report No. 2000-02, NOAA/NESDIS, National Climatic Data Center, Ashville, NC.

Namias, J., 1991: Spring and summer 1988 drought over the contiguous United States—Causes and prediction. *J. Climate*, **4**, 54–65.

Ross T. and N. Lott, 2003: A Climatology of 1980-2003 Extreme Weather and Climate Events. Technical Report No. 2003-01, NOAA/NESDIS, National Climate Data Center, Ashville, NC.

McCabe, G. J., M. A. Palecki, and J. L. Betancourt, 2004: Pacific and Atlantic Ocean influences on multidecadal drought frequency in the United States. *Proceedings of the National Academy of Sciences*, **101**, 4136-4141.

Molod, A., L. Takacs, M. Suarez, J. Bacmeister, I.-S. Song, and A. Eichmann, 2012: The GEOS-5 atmospheric general circulation model: Mean climate and development from MERRA to Fortuna. NASA Tech. Rep. Series on Global Modeling and Data Assimilation, Vol. 28, NASA TM–2012-104606, 117 pp.

Moorthi, S., and M. J. Suarez, 1992: Relaxed Arakawa-Schubert: A parameterization of moist convection for general circulation models. *Mon. Wea. Rev*., **120**, 978–1002.

Nigam, S., B. Guan, and A. Ruiz-Barradas, 2011: Key role of the Atlantic Multidecadal Oscillation in 20th century drought and wet periods over the Great Plains, *Geophys. Res. Lett*., **38**, L16713, doi:10.1029/2011GL048650.

Peña, Malaquías, Ming Cai, Eugenia Kalnay, 2004: Life Span of Subseasonal Coupled Anomalies. *J. Climate*, **17**, 1597–1604.

Reichle, R. H., R. D. Koster, G. J. M. De Lannoy, B. A. Forman, Q. Liu, S. P. P. Mahanama, and A. Toure, 2011: Assessment and enhancement of MERRA land surface hydrology estimates. *J. Climate*, **24**, 6322-6338.

Richman, M. B., 1986: Rotation of principal components. *Int. J. Climatol.*, **6**, 293–335.

Rienecker, M. M., and Coauthors, 2008: The GEOS-5 Data Assimilation System—Documentation of versions 5.0.1, 5.1.0, and 5.2.0. Tech. Rep. Series on Global Modeling and Data Assimilation, Vol. 27, NASA/TM-2008-104606, 95 pp.

Rienecker, M. M., and Coauthors, 2011: MERRA—NASA's Modern-Era Retrospective Analysis for Research and Applications. *J. Climate*, **24**, 3624–3648.

Schubert, S.D., M. J. Suarez, P. J. Pegion, R. D. Koster, and J. T. Bacmeister , 2004: On the Cause of the 1930s Dust Bowl, *Science*, **33**, 1855-1859.

Schubert S., H. Wang and co-authors, 2009: A USCLIVAR project to assess and compare the responses of global climate models to drought-related SST forcing patterns: Overview and results. *J. Climate*, **22**, 5251-5272.

Schubert, Siegfried, Hailan Wang, and Max Suarez, 2011: Warm Season Subseasonal Variability and Climate Extremes in the Northern Hemisphere: The Role of Stationary Rossby Waves. *J. Climate*, **24**, 4773–4792.

Schubert, Siegfried D., Hailan Wang, Randal D. Koster, Max J. Suarez, and Pavel Ya. Groisman, 2014: Northern Eurasian Heat Waves and Droughts. *J. Climate*, **27**, 3169–3207.

Schubert S. and co-authors, 2015: Global Drought: A Synthesis of Current Understanding with a Focus on Precipitation. *J. Climate*. Submitted.

Seager, R., Y. Kushnir, C. Herweijer, N. Naik, and J. Velez, 2005: Modeling the tropical forcing of persistent droughts and pluvials over western North America: 1856-2000. *J. Climate*, **18**, 4068-4091.

Seager, R. and M. Hoerling, 2014: Atmosphere and Ocean Origins of North American Drought. *J. Climate*, **27**, 4581-4606.

Smith, A., and R. Katz, 2013: U.S. Billion-dollar Weather and Climate Disasters: Data Sources, Trends, Accuracy and Biases. *Natural Hazards*. DOI: 10.1007/s11069-013-0566-5.

Ting, Mingfang, Hui Wang, 1997: Summertime U.S. Precipitation Variability and Its Relation to Pacific Sea Surface Temperature. *J. Climate*, **10**, 1853–1873.

Wang H., S. Schubert, M. Suarez and R. Koster, 2010: The physical mechanisms by which the leading patterns of SST variability impact U.S. precipitation. *Journal of Climate*, **23**, 1815-1836.

Wang, Yafei, Anthony R. Lupo, 2009: An Extratropical Air–Sea Interaction over the North Pacific in Association with a Preceding El Niño Episode in Early Summer. *Mon. Wea. Rev.*, **137**, 3771–3785.

Table 1. The list of experiments performed for a stationary Rossby wave event that developed during 20 May – 15 June 1988 using the NASA GEOS-5 AGCM and MERRA. The experiments A1-A2 and B1-B4 are used to study the processes that affect stationary Rossby waves and their effects over North America. These processes include (A) the 21z 20 May 1988 atmospheric and land initial conditions, (B) the 21z 20 May 1988 land initial conditions, (C) observed stationary wave sources over western Pacific, (D) soil moisture feedback, and (E) corrected model mean jet over north Pacific. The experiment C1 is used to investigate the connections between the 1988 North American drought and surface anomalies developed over northern Eurasia about two to three weeks later. Each experiment consists two sets of ensembles, a control ensemble and an anomaly ensemble. The control ensemble consists of 31 members for years 1980 through 2010 forced with the 1988 observed SST, initialized using MERRA conditions for years 1980-2010. The anomaly ensemble consists of 30 members for year 1988 forced with observed SST. The atmospheric and land initial conditions used vary in the experiments. All experiments are run through the end of July, at a horizontal resolution of 1° latitude/longitude.

Experiments	**Replay region**	**Replay variables**	**Atmospheric and land initial conditions**	**Land feedback**	**Processes**
A1	N/A	N/A	*Control*: 21z, 20 May of 1980-2010 *Anomaly*: 21z, 20 May 1988 plus small atmospheric perturbations	Yes	A
A2	N/A	N/A	*Control:* same as A1 *Anomaly:* 21z, 20 May of 1980-2009 for atmosphere; 21z, 20 May 1988 for land	Yes	B
B1	90°E-140°E; 0°-70°N	U,V,T,Q,Ps	Same as A1	Yes	A, C, D, E
B2			*Control*: 21z, 2 May of 1980-2010 *Anomaly*: 21z, 2 May of 1980-2009	Yes	C, D, E
B3			Same as B2	No	C, E
B4		U,V	Same as B2	Yes	C, D
C1	130°W-70°W; 0°-70°N	U,V,T,Q,Ps	Same as B2	Yes	C, D, E

Figures

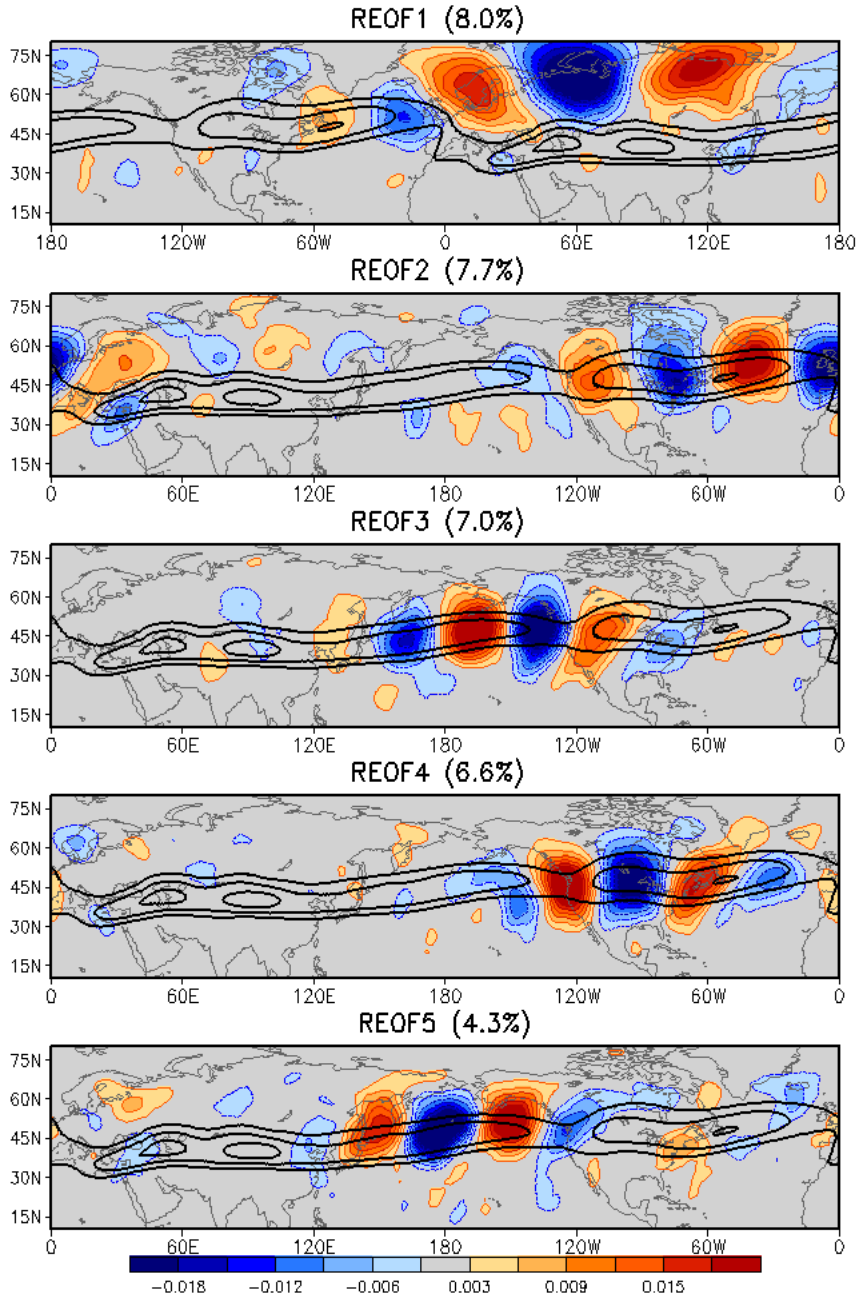

Figure 1. The leading REOFs of MERRA 250-hPa intraseasonal monthly mean meridional wind anomalies for JJA of 1980–2014. Units are arbitrary. The thick black contours are the long-term JJA mean (1980–2010) 250-hPa zonal wind at 15, 20, 25 m s^{-1}. Note that the central longitude in the panel for REOF1 is 180°E, whereas it is 0ºE for the other REOFs.

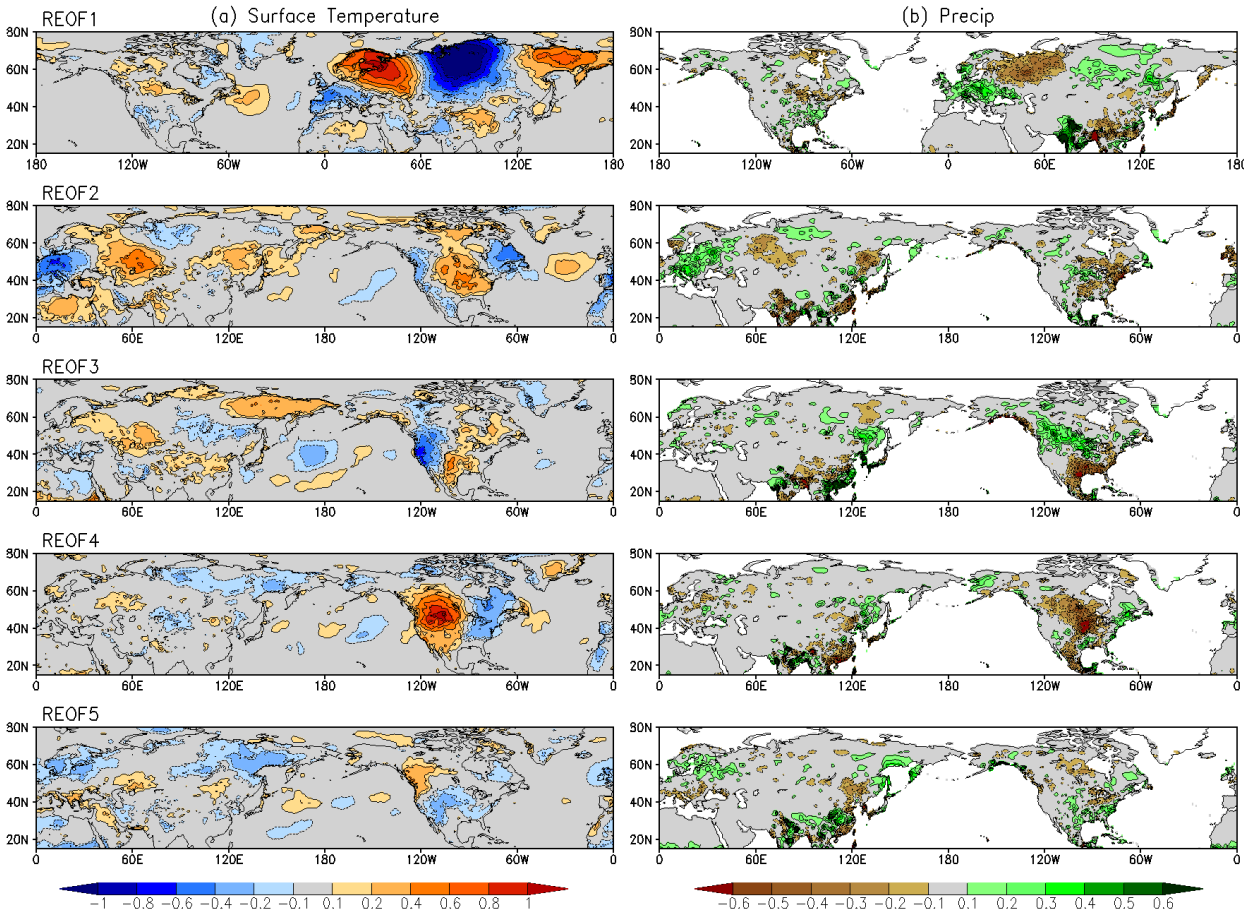

Figure 2. The subseasonal anomalies of (a) MERRA surface temperature (K), and (b) MERRA-Land precipitation (mm day^{-1}) associated with the five leading REOFs of MERRA 250-hPa subseasonal meridional wind anomalies, based on a linear regression against the normalized RPCs of these leading REOFs for JJA of 1980–2014.

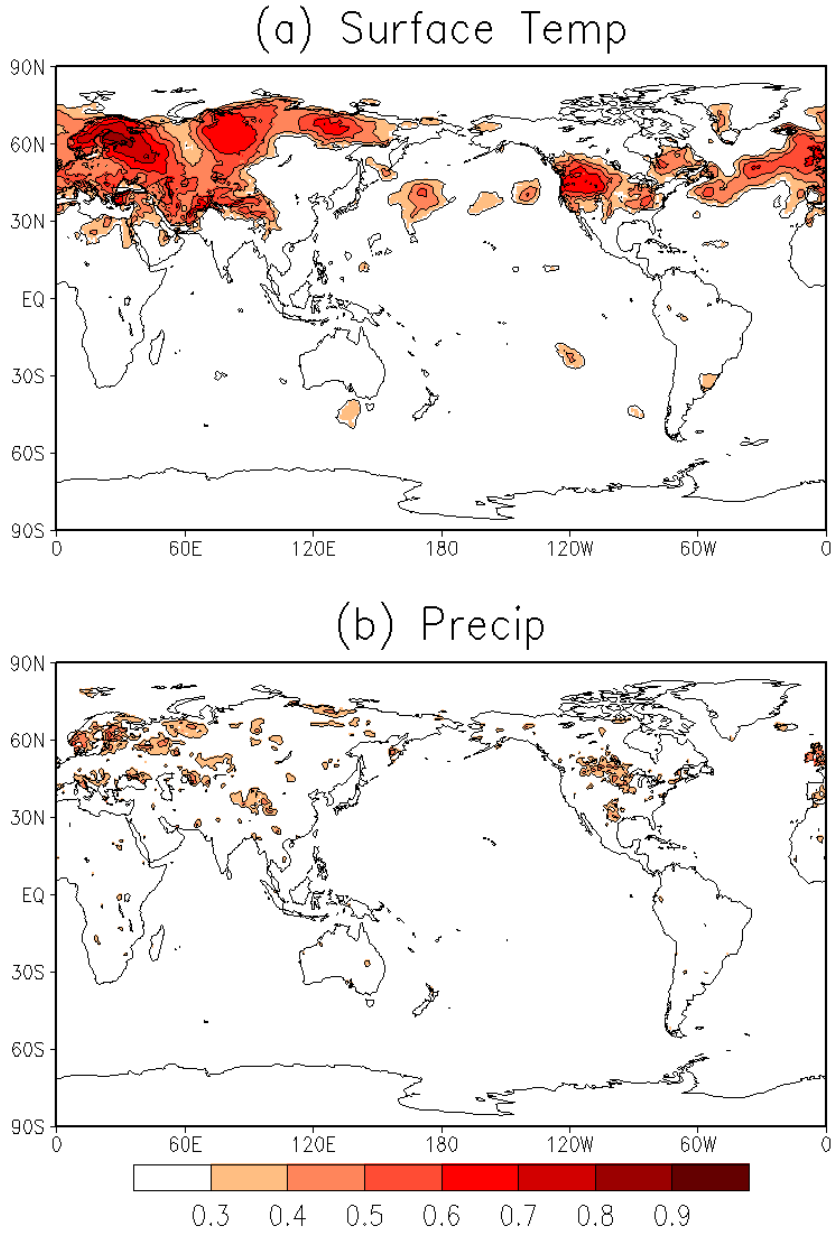

Figure 3. The spatial distribution of the fraction of monthly (JJA1980–2014) subseasonal variance of (a) surface temperature and (b) precipitation explained by the first ten 250-hPa subseasonal meridional wind REOFs, based on a linear regression. Contours start at 0.3 with a 0.1 interval. Shaded values are significant at the 5% (10%) level for surface temperature (precipitation) based on a Monte Carlo test.

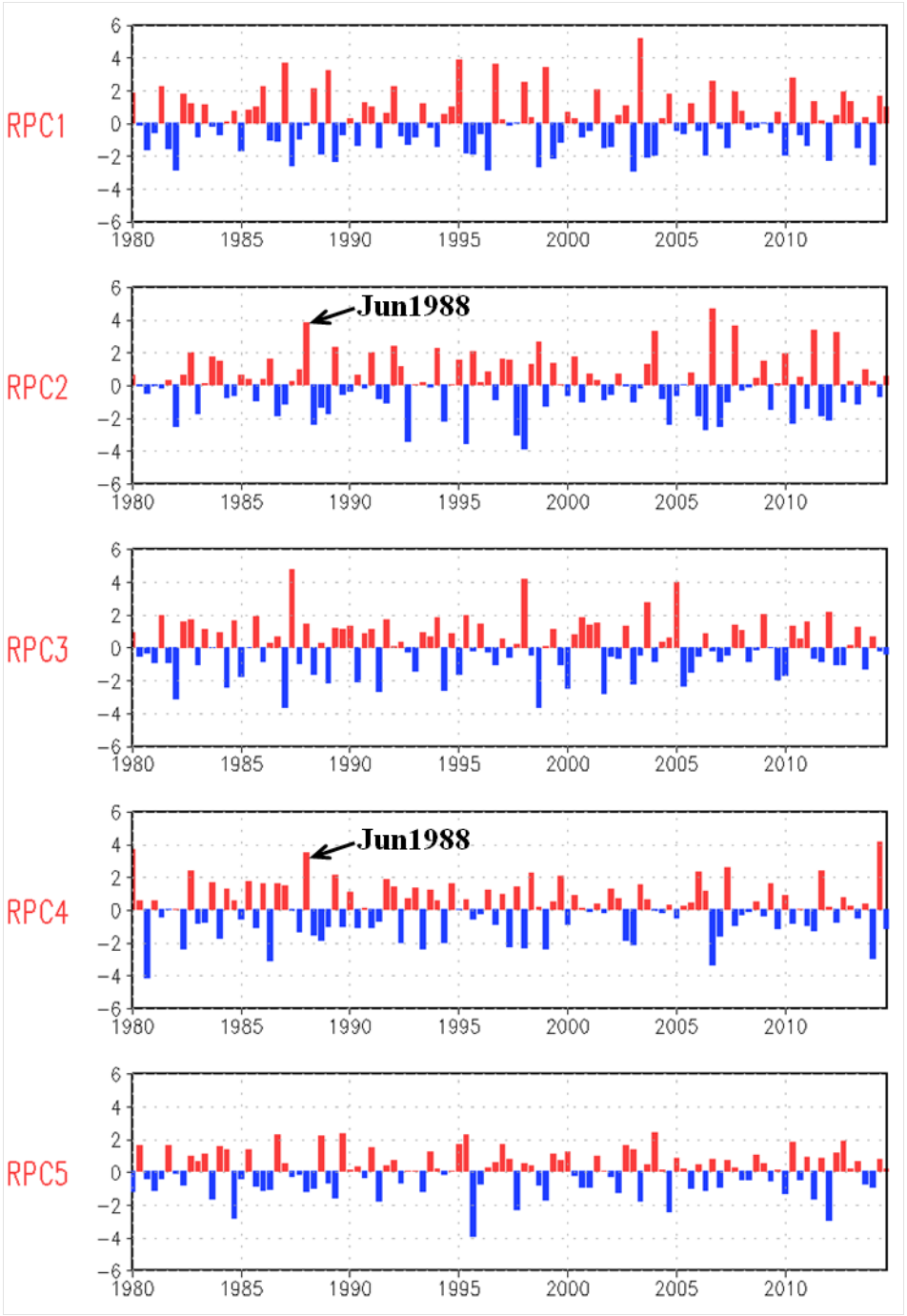

Figure 4. The leading RPCs of MERRA 250-hPa subseasonal monthly mean meridional wind anomalies for June, July and August of 1980–2014.

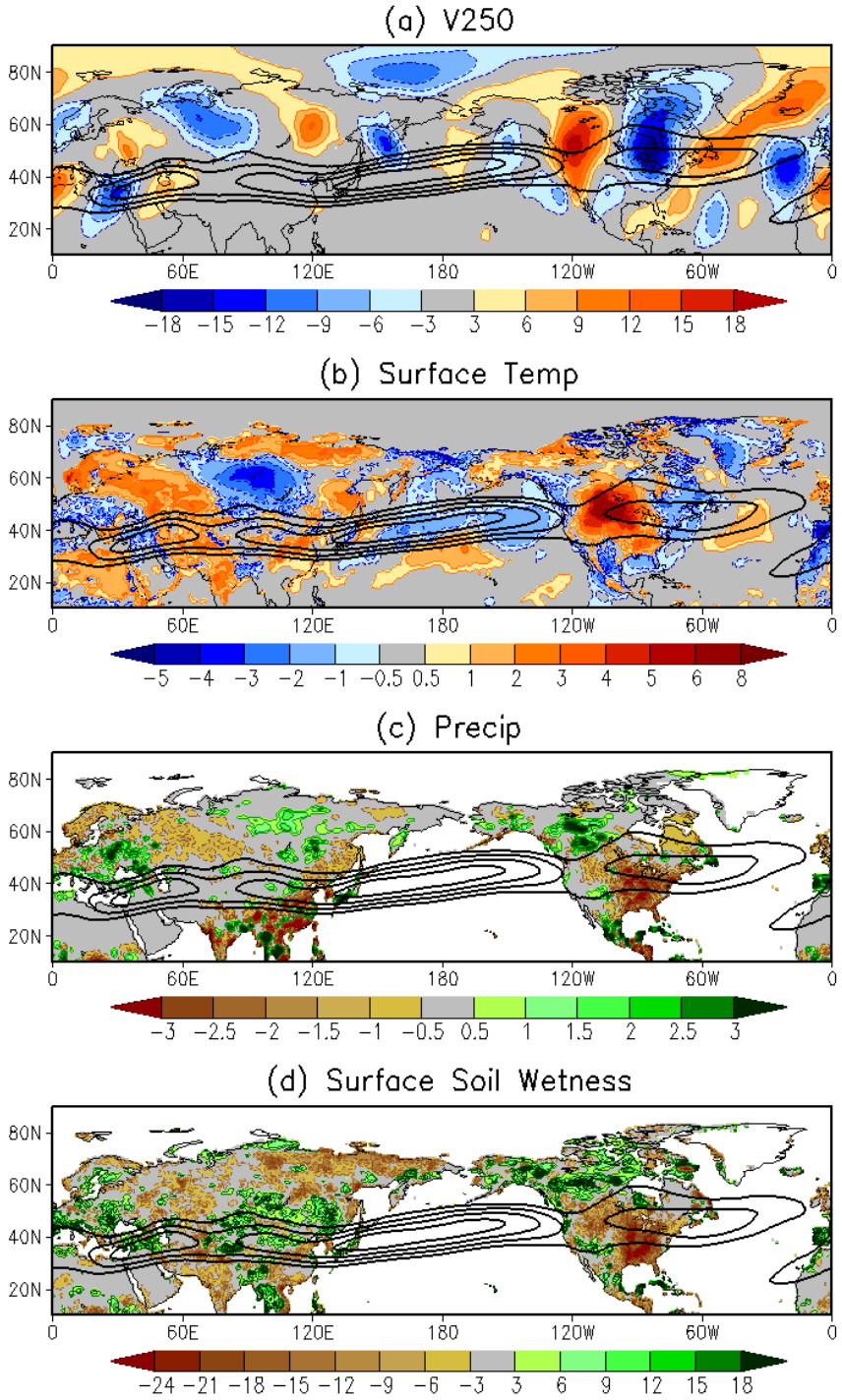

Figure 5. The June 1988 monthly anomalies for (a) MERRA 250-hPa meridional wind (m s^{-1}), (b) MERRA surface temperature (K), (c) MERRA-Land precipitation (mm day^{-1}) and (d) MERRA-Land surface soil wetness (%). These anomalies are obtained as deviations from their 1980-2010 monthly means. The contours show the long-term mean (1980-2010) of June 250-hPa zonal wind, starting at 15 m s^{-1} with a 5 m s^{-1} interval.

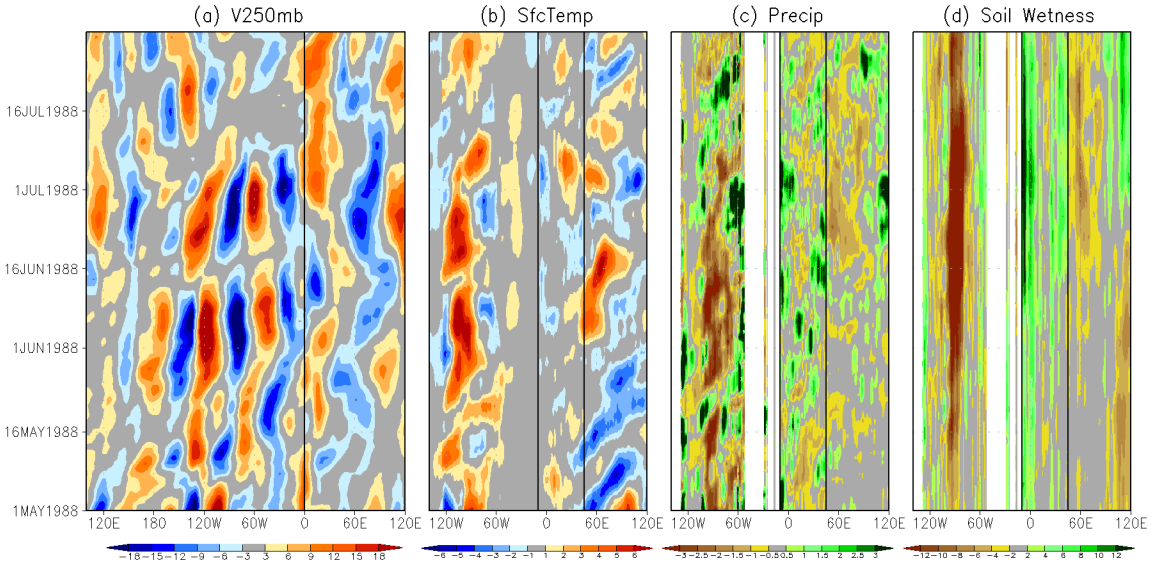

Figure 6. Evolution of (a) MERRA daily 250-hPa meridional wind (m s^{-1}) averaged between 40ºN-60ºN west of 0º and 50ºN-70ºN east of 0º, with a 10-day running mean smoother applied, (b) MERRA daily surface temperature anomalies (K), (c) MERRA-Land daily precipitation anomalies (mm day^{-1}), and (d) MERRA-Land daily surface soil wetness anomalies (%), averaged between 30ºN-50ºN west of 10ºW, between 35ºN-55ºN for 10ºW-45ºE, and between 50ºN-70ºN east of 45ºE, with a 5-day running mean smoother applied, during the period 1 May – 31 July 1998.

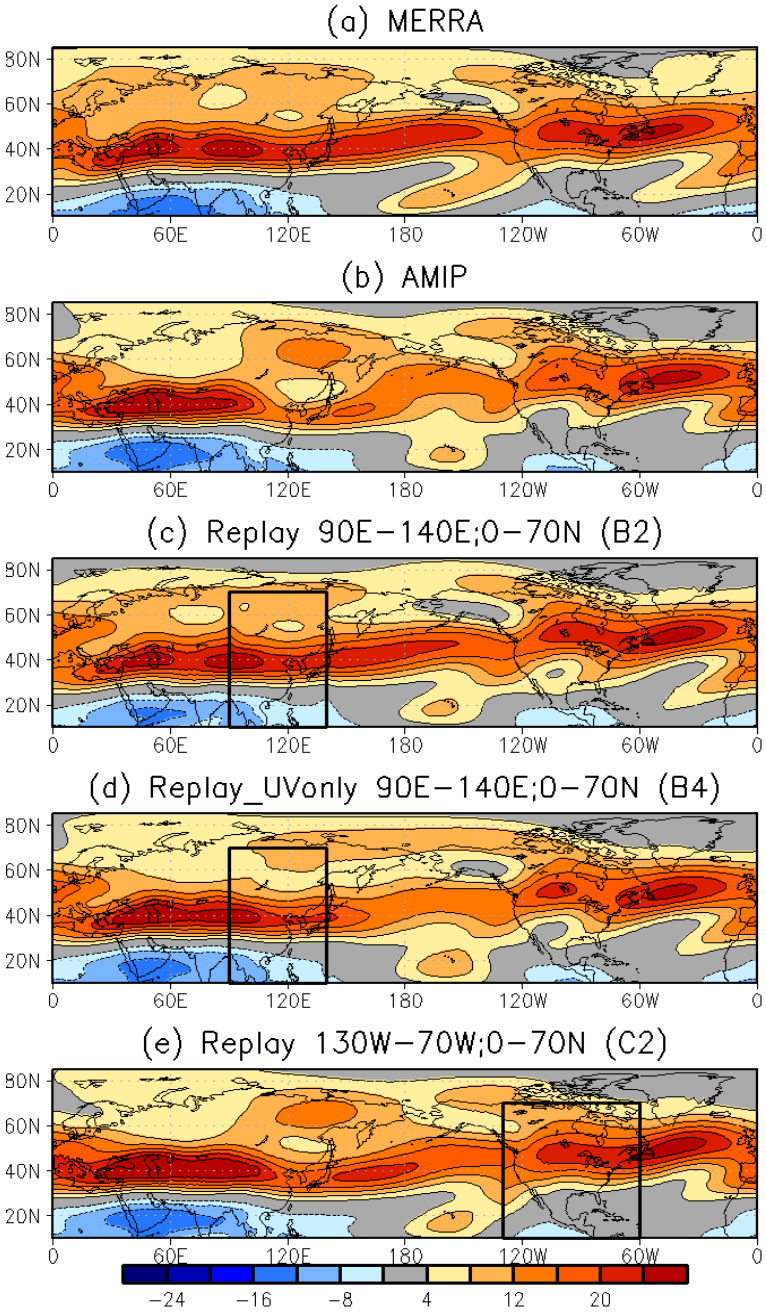

Figure 7. The long-term mean (1980-2010) of JJA 250-hPa zonal wind (m s^{-1}) in (a) MERRA, (b) the GEOS-5 AMIP simulations, (c) the GEOS-5 AGCM regional replay experiment in which the model atmosphere is constrained to be close to MERRA over eastern Asia and the western Pacific (90°E-140°E; 0°-70°N) (experiment B2), (d) same as (c) except that only zonal and meridional wind fields are replayed (experiment B4), (e) same as (c) except for the AGCM regional replay experiment over North America (130°W-70°W; 0°-70°N) (experiment C1). The portions of the replay regions in the plotting domain are indicated using black boxes.

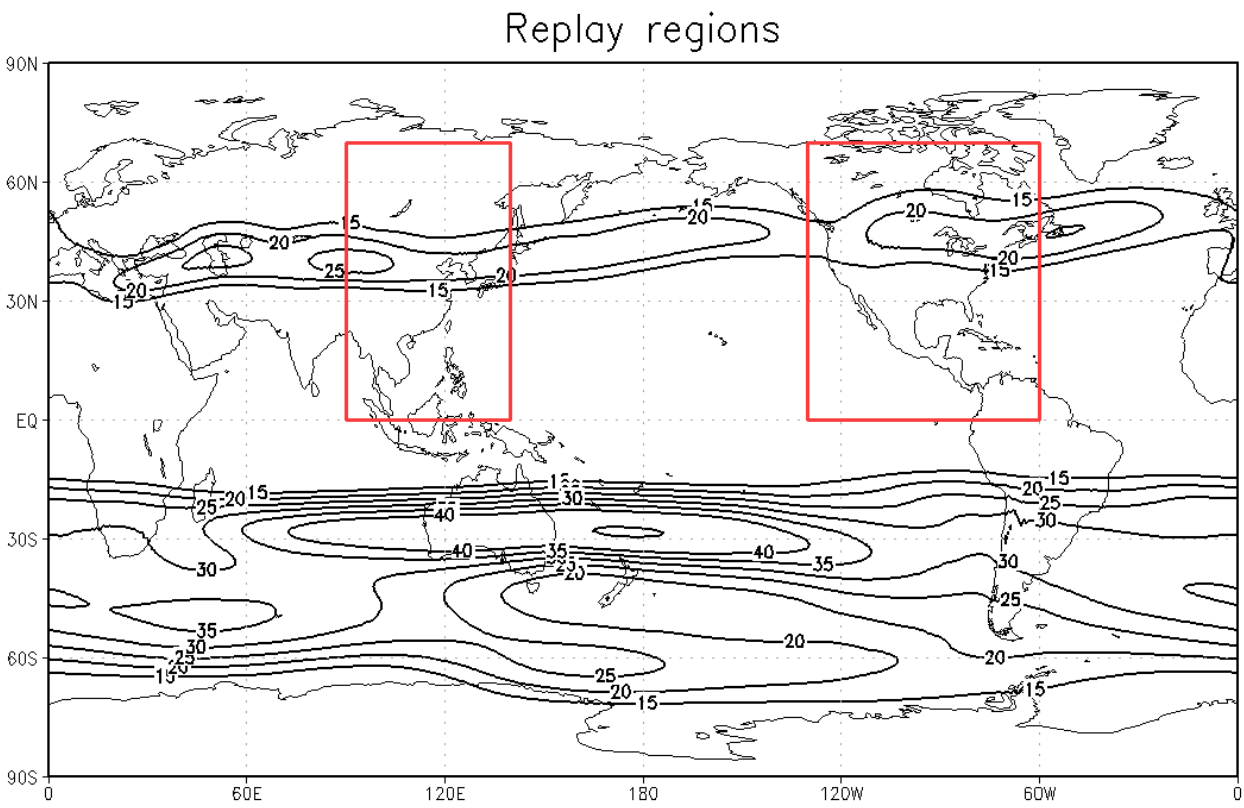

Figure 8. The regions of eastern Asia and the western Pacific (90°E-140°E, 0-70°N) and North America (230°E-290°E, 0-70°N) used in the GEOS-5 AGCM regional replay experiments. The contours show the long-term mean (1980-2010) of JJA 250-hPa zonal wind from MERRA, starting from 15 m s^{-1} with a 5 m s^{-1} interval.

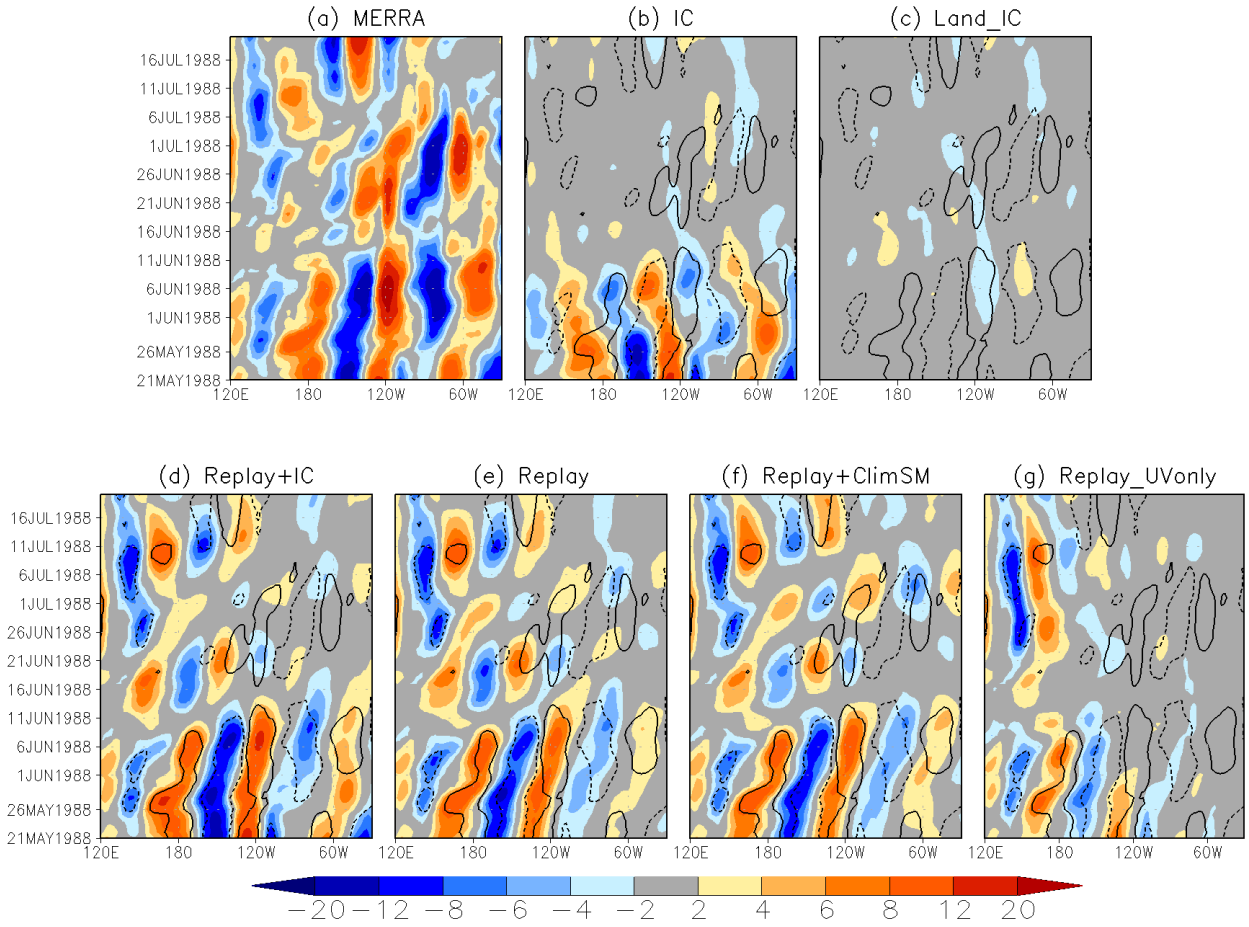

Figure 9. Evolution of daily 250-hPa meridional wind component (m s^{-1}) averaged between 30ºN-60ºN with a 10-day running mean smoother applied in (a) MERRA, (b) the ensemble mean of the GEOS-5 AGCM hindcast initialized using MERRA atmospheric and land conditions at 21z 20 May 1988 (experiment A1), (c) same as (b) but for the AGCM hindcast that uses MERRA atmospheric conditions at 21z 20 May of years 1980-2009 to initialize the atmosphere of its anomaly ensemble (experiment A2), (d) the ensemble mean of the GEOS-5 AGCM regional replay over eastern Asia and the western Pacific (90ºE-140ºE, 0º-70ºN) initialized using MERRA atmospheric and land conditions at 21z 20 May, 1988 (experiment B1), (e) same as (d) but initialized using MERRA atmospheric and land conditions at 21z 2 May of years 1980-2009 (experiment B2), (f) same as (e) but have land feedback disabled (experiment B3), and (g) same as (e) but replay only zonal and meridional wind fields (experiment B4). The black contours in (b)-(g) indicate the -6 m s^{-1} and 6 m s^{-1} contours of MERRA in (a).

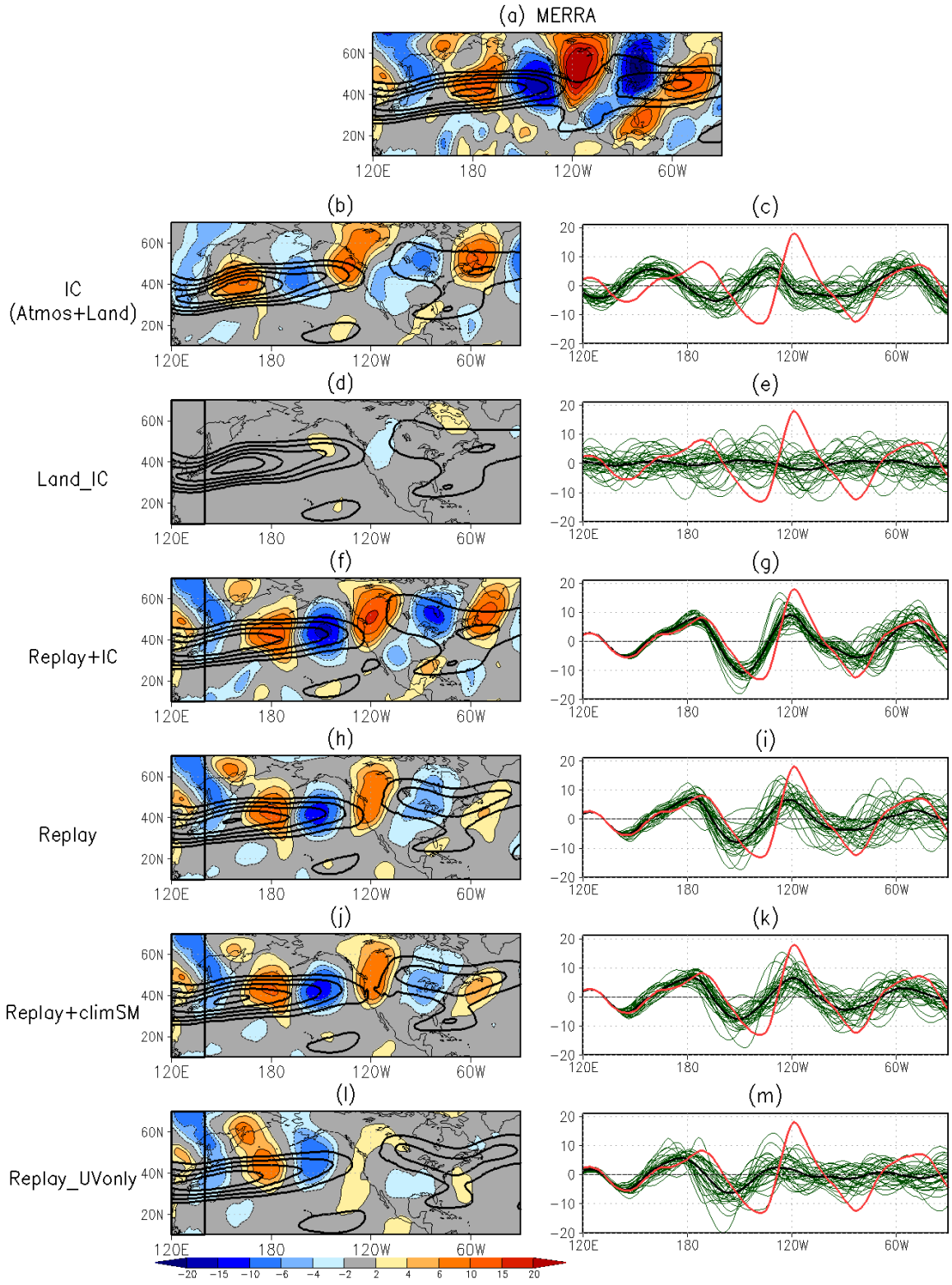

Figure 10. The 250-hPa meridional wind anomalies (m s^{-1}) averaged over the period 26 May – 10 June 1988 in (a) MERRA, (b) the ensemble mean of the GEOS-5 AGCM hindcast initialized using MERRA atmospheric and land conditions at 21z 20 May 1988 (experiment A1), (c) the

mean 250-hPa meridional wind response over the period 26 May – 10 June 1988 averaged over 30°N-60°N in the 30 ensemble members (thin green lines) and their ensemble mean (thick black line) in the AGCM hindcast (experiment A1), and the corresponding anomalies in MERRA (thick red line), (d)-(e) same as (b)-(c) but for the AGCM hindcast initialized using MERRA atmospheric conditions at 21z 20 May of years 1980-2009, and MERRA land conditions at 21z 20 May 1988 (experiment A2), (f)-(g) same as (b)-(c) but for the AGCM regional replay experiment over eastern Asia and the western Pacific (90°E-140°E, 0°-70°N) initialized using MERRA atmospheric and land conditions at 21z 20 May 1988 (experiment B1), (h)-(i) same as (f)-(g) but initialized using MERRA atmospheric and land conditions at 21z 2 May of years 1980-2009 (experiment B2), (j)-(k) same as (h)-(i) but have land feedback disabled (experiment B3), (l)-(m) same as (h)-(i) but replay only zonal and meridional wind (experiment B4). The black contours in (a), (b), (d), (f), (h), (j) and (l) indicate the 250-hPa zonal wind (m s^{-1}) averaged over 28 May – 15 June 1988 in MERRA and the AGCM experiments; they start at 15 m s^{-1} with a 5 m s^{-1} interval.

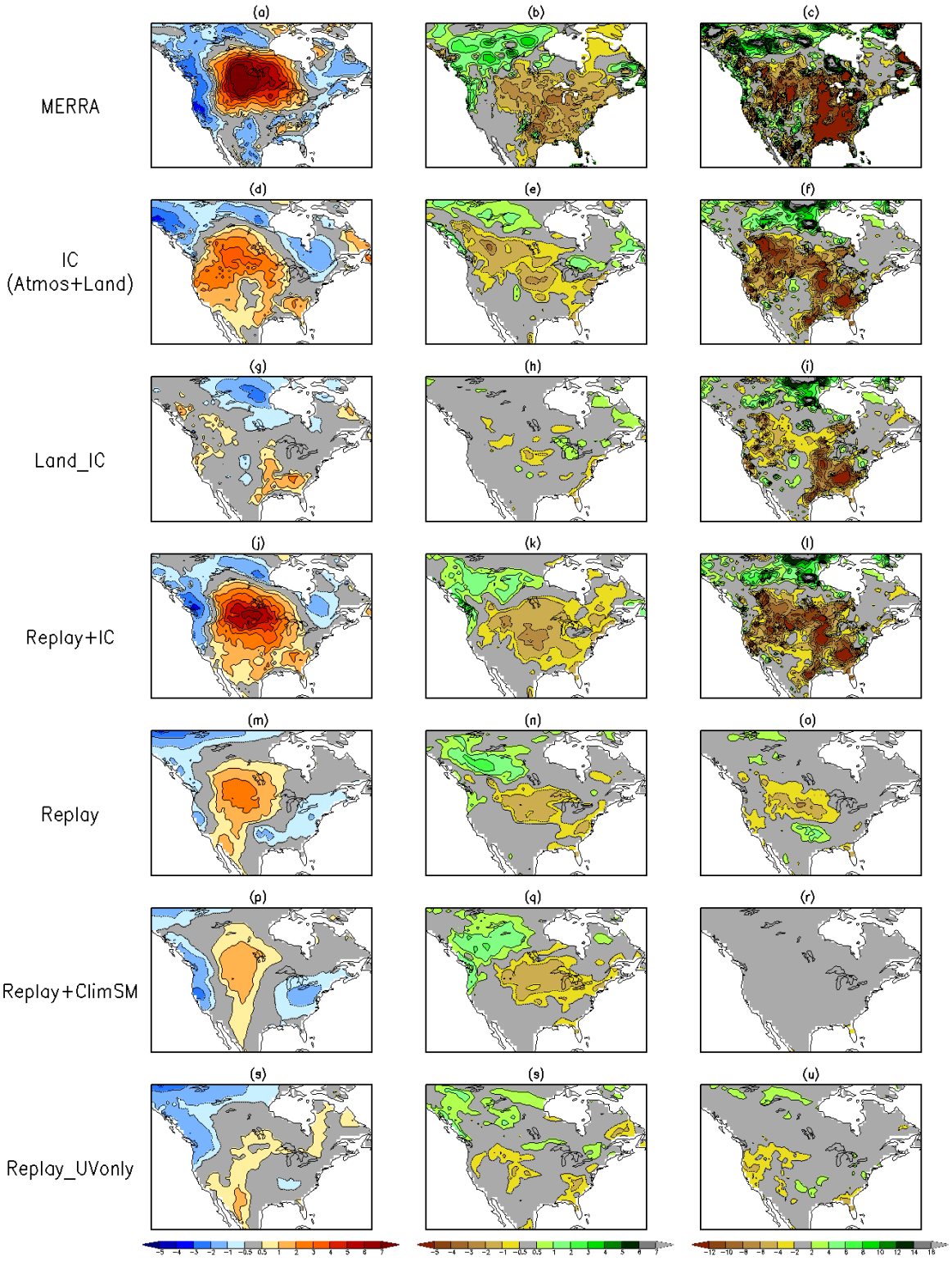

Figure 11. The anomalies of (a) MERRA surface temperature (K), (b) MERRA-Land precipitation (mm day^{-1}), and (c) MERRA-Land surface soil wetness (%) averaged over the period 26 May – 10 June 1988; (d)-(f) same as (a)-(c) but for the GEOS-5 AGCM hindcast

initialized using MERRA atmospheric and land conditions at 21z 20 May 1988 (experiment A1); (g)-(i) same as (a)-(c) but for the GEOS-5 AGCM hindcast initialized using MERRA atmospheric conditions at 21z 20 May of years 1980-2009, and MERRA land conditions at 21z 20 May 1988 (experiment A2); (j)-(l) same as (a)-(c) but for the GEOS-5 AGCM regional replay over eastern Asia and the western Pacific (90ºE-140ºE;0º-70ºN) initialized using MERRA atmospheric and land conditions at 21z 20 May 1988 (experiment B1); (m)-(o) same as (j)-(l) but initialized using MERRA atmospheric and land conditions at 21z 2 May of years 1980-2009 (experiment B2); (p)-(r) same as (m)-(o) but have land feedback disabled (experiment B3); (s)-(u) same as (m)-(o) but replay only zonal and meridional wind over eastern Asia and the western Pacific (90ºE-140ºE;0º-70ºN) (experiment B4).

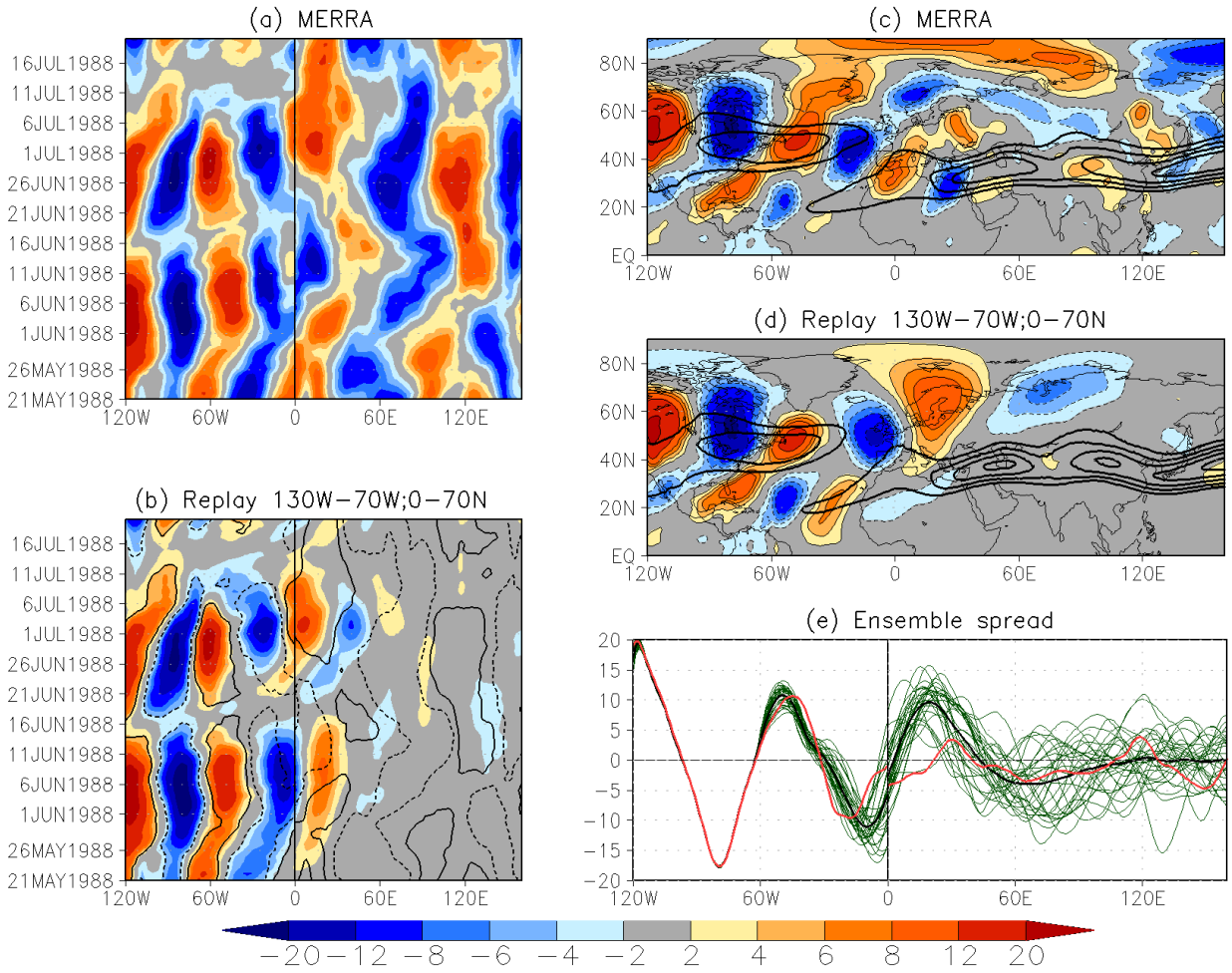

Figure 12. The 250-hPa meridional wind anomalies (m s^{-1}) averaged over 40ºN-60ºN west of 0º and 50ºN-70ºN east of 0º, with 10-day running mean applied in (a) MERRA and (b) the ensemble mean of the regional replay experiment in which the model atmosphere is constrained to be close to MERRA over North America (130ºW-70ºW;0°-70°N) (experiment C1); the 250-hPa meridional wind anomalies averaged over 28 May – 15 June 1988 in (c) MERRA, (d) the ensemble mean of the regional replay experiment over North America (experiment C1); (e) the mean 250-hPa meridional wind anomalies over 28 May – 15 June 1988 averaged over 40ºN-60ºN west of 0º and 50ºN-70ºN east of 0º, in the 30 ensemble members (thin green lines), the 30-member ensemble mean (thick black line), and MERRA (thick red line). The black contours in (b) indicate the -6 m s^{-1} and 6 m s^{-1} contours of MERRA in (a). The black contours in (c) and (d) indicate the 250-hPa zonal wind (m s^{-1}) averaged over 28 May – 15 June 1988 in MERRA and experiment C1, starting at 15 m s^{-1} with a 5 m s^{-1} interval.

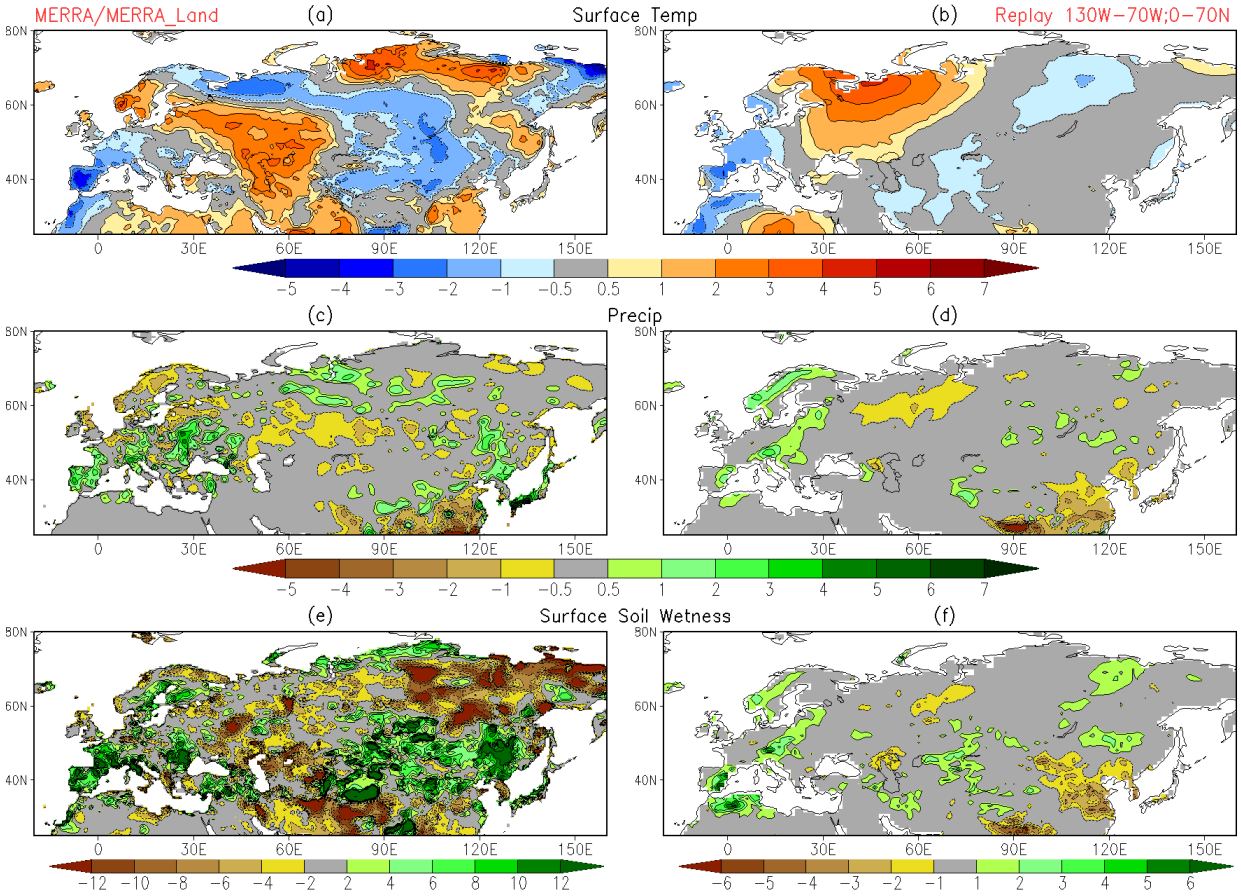

Figure 13. The surface temperature anomalies (K) averaged over the period 28 May – 15 June 1988 in (c) MERRA, and (b) the ensemble mean of the AGCM regional replay experiment over North America (130ºW-70ºW;0°-70°N) (experiment C1); (c) same as (a) but for MERRA-Land precipitation (mm day^{-1}); (d) same as (b) but for precipitation (mm day^{-1}); (e)-(f) same as (c)-(d) but for surface soil wetness (%).

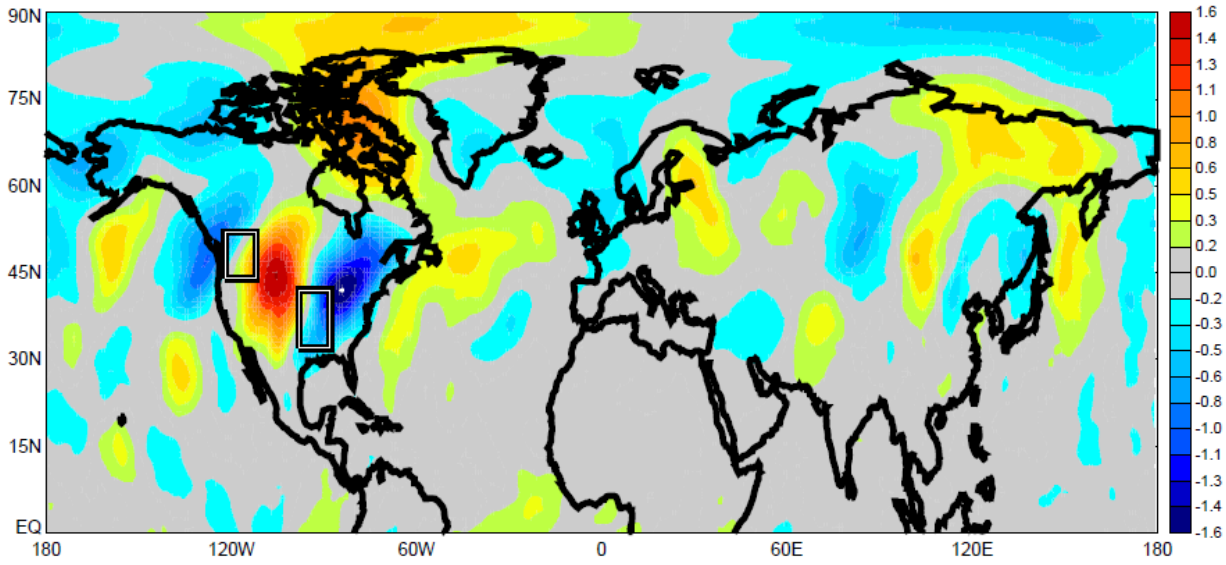

Figure 14. Results from Koster et al. (2014): The July 250-hPa meridional wind modifications (relative to a control) produced by an experiment in which wet and dry soil moisture anomalies were imposed in the northwest U.S. and southern Great Plains, respectively (see indicated rectangles).